Manuscript prepared for Atmos. Chem. Phys.
with version 1.3 of the LaTeX class copernicus.cls.
Date: 5 March 2010

Optimal estimation retrieval of aerosol microphysical properties from SAGE II satellite observations in the volcanically unperturbed lower stratosphere

D. Wurl[1], R. G. Grainger[2], A. J. McDonald[1], and T. Deshler[3]

[1]Department of Physics and Astronomy, University of Canterbury, Christchurch, New Zealand
[2]Department of Atmospheric, Oceanic and Planetary Physics, University of Oxford, Oxford, UK
[3]Department of Atmospheric Science, College of Engineering, University of Wyoming, Laramie, USA

Correspondence to: D. Wurl (daniela_wurl@yahoo.de)

Abstract.

Stratospheric aerosol particles under non-volcanic conditions are typically smaller than 0.1 µm. Due to fundamental limitations of the scattering theory in the Rayleigh limit, these tiny particles are hard to measure by satellite instruments. As a consequence, current estimates of global aerosol properties retrieved from spectral aerosol extinction measurements tend to be strongly biased. Aerosol surface area densities, for instance, are observed to be about 40% smaller than those derived from correlative in situ measurements (Deshler et al., 2003). An accurate knowledge of the global distribution of aerosol properties is, however, essential to better understand and quantify the role they play in atmospheric chemistry, dynamics, radiation and climate.

To address this need a new retrieval algorithm was developed, which employs a nonlinear Optimal Estimation (OE) method to iteratively solve for the monomodal size distribution parameters which are statistically most consistent with both the satellite-measured multi-wavelength aerosol extinction data and a priori information. By thus combining spectral extinction measurements (at visible to near infrared wavelengths) with prior knowledge of aerosol properties at background level, even the smallest particles are taken into account which are practically invisible to optical remote sensing instruments.

The performance of the OE retrieval algorithm was assessed based on synthetic spectral extinction data generated from both monomodal and small-mode-dominant bimodal sulphuric acid aerosol size distributions. For monomodal background aerosol, the new algorithm was shown to fairly accurately retrieve the particle sizes and associated integrated properties (surface area and volume densities), even in the presence of large extinction uncertainty. The associated retrieved uncertainties are a good estimate of the true errors. In the case of bimodal background aerosol, where the

retrieved (monomodal) size distributions naturally differ from the correct bimodal values, the associated surface area (A) and volume densities (V) are, nevertheless, fairly accurately retrieved, except at values larger than $1.0\,\mu m^2 cm^{-3}$ (A) and $0.05\,\mu m^3 cm^{-3}$ (V), where they tend to underestimate the true bimodal values. Due to the limited information content in the SAGE II spectral extinction measurements this kind of forward model error cannot be avoided here. Nevertheless, the retrieved uncertainties are a good estimate of the true errors in the retrieved integrated properties, except where the surface area density exceeds the $1.0\,\mu m^2 cm^{-3}$ threshold.

When applied to near-global SAGE II satellite extinction measured in 1999 the retrieved OE surface area and volume densities are observed to be larger by, respectively, 20–50% and 10–40% compared to those estimates obtained by the SAGE II operational retrieval algorithm. An examination of the OE algorithm biases with in situ data indicates that the new OE aerosol property estimates tend to be more realistic than previous estimates obtained from remotely sensed data through other retrieval techniques.

Based on the results of this study we therefore suggest that the new Optimal Estimation retrieval algorithm is able to contribute to an advancement in aerosol research by considerably improving current estimates of aerosol properties in the lower stratosphere under low aerosol loading conditions.

1 Introduction

Stratospheric aerosols are known to play an important role in the climate system because they can influence the global chemical and radiation balance in the atmosphere in a number of ways (McCormick et al., 1995; Solomon, 1999). In the aftermath of large volcanic eruptions stratospheric aerosols have a significant impact on the Earth's radiation balance for several years after the eruption. The observation that stratospheric sulphuric acid aerosol can exert a cooling effect on tropospheric temperatures (e.g. Pueschel, 1996) has even stimulated the idea of deliberately introducing aerosols to counteract climate warming caused by anthropogenic emissions of greenhouse gases. This area of research, called geoengineering by sulphate aerosols, is receiving increasing attention (e.g. Rasch et al., 2008a,b; Tilmes et al., 2008). During volcanically quiescent periods, when stratospheric aerosol can be characterized as in a background state unperturbed by volcanism, the direct radiative impact of stratospheric aerosols tends to be rather small. However, these particles may also play a role in the nucleation of near tropopause cirrus, and thus indirectly affect radiation (Kärcher and Ström, 2003; Penner et al., 2009). Stratospheric background aerosols also play an important role in the chemical balance of the stratosphere. At mid-latitudes they affect the ozone balance indirectly by interacting with both nitrous oxides (Fahey et al., 1993) and chlorine reservoir species. For instance, NO_x increases under low aerosol loading conditions and induces ozone loss from the nitrogen catalytic cycle (Crutzen, 1970). In the polar stratosphere the small aerosol particles provide condensation sites for polar stratospheric clouds which then provide the surfaces necessary to con-

vert inactive to active chlorine leading to polar ozone loss. These examples provide an insight into the intricate interactions between stratospheric aerosols and the climate system.

The impact of an aerosol on the different processes is determined by the chemical composition and, more importantly, by the microphysical properties: particle size distribution, surface area density, and the volume density. These properties are determined by the production mechanisms of the particles, by the source of precursor gases and subsequent chemical reactions, by temperature and the abundance of gas phase sulphuric acid, and by the growth and removal processes.

Much knowledge about these aspects was gained from in situ measurements. The stratospheric aerosol layer was first measured in the late 1950s using balloon-borne impactors (Junge et al., 1961) and is often called the Junge layer, although its existence was suggested 50 years earlier from twilight observations (Gruner and Kleinert, 1927). From a number of complementary measurements the knowledge was established that stratospheric aerosol is composed primarily of sulphuric acid and water during both volcanically active and quiescent periods (e.g. Junge et al., 1961; Rosen, 1971; Hofmann and Rosen, 1961; Deshler et al., 1992; Sheridan et al., 1992; Grainger at al., 1993; Arnold et al., 1998; Murphy et al., 1998). Under background conditions, these originate mainly from the tropospheric source gases carbonyl sulphide (OCS), (an inert sulphur bearing molecule), and SO_2, and from direct injections of sulphate particles (Crutzen, 1976; Turco et al., 1980; Weisenstein and Bekki , 2006). During strong volcanic eruptions, sulphur is directly injected into the stratosphere and then oxidized and transformed into sulphuric acid. Other minor constituents of stratospheric aerosol include upper tropospheric material such as nitrate, ammonia, organics, minerals and metals (e.g. Talbot et al., 1998; Murphy et al., 1998), or meteoric material (Murphy et al., 2007; Renard et al., 2008), aircraft and rocket exaust (Kjellstrom et al., 1999; Danilin et al., 2001; Jackman et al., 1996). A comprehensive review of the measurements, the importance, and the life cycle of local and global stratospheric aerosol can be found in Deshler (2008).

Direct measurements of size resolved particle concentrations in the lower stratosphere are provided by balloon-borne in situ measurements which are limited primarily to Laramie/Wyoming/USA (41° N) with sporadic measurements from Lauder/NZ (45° S) and a few other locations (Hofmann et al., 1975; Deshler et al., 2003). These measurements will be used (in this study) as prior knowledge, with the help of which SAGE II spectral extinction measurements will be evaluated to obtain new estimates of aerosol properties under non-volcanic conditions. The balloone-borne measurements from Laramie (Deshler et al., 2003) along with ground based lidar measurements at two mid-latitude sites (Osborn et al., 1995; Jäger, 2005) and two tropical sites (Barnes and Hofmann, 1997; Simonich and Clemesha, 1997) provide the longest stratospheric aerosol records available (Deshler et al., 2006). They are particularly valuable, for instance, for having captured the complete cycle of three major volcanic eruptions (Fuego, 1974, 14° N; El Chichón, 1982, 17° N; Pinatubo, 1991, 15° N) which have not been measured in as much detail or even not at all by satellite instruments.

Although ground-based or air-borne in situ measurements provide detailed and valuable infor-

mation about stratospheric aerosol properties, their reach remains local. To be able to quantify the climatic impact of stratospheric aerosol on a global scale, they have to be complemented by large-scale measurements from space based platforms.

Long-term measurements of the global stratospheric aerosol burden using satellite instruments began in the late 1970s with the Stratospheric Aerosol Measurement (SAM) II (Pepin et al., 1977; Poole and Pitts, 1994) and the Stratospheric Aerosol and Gas Experiment (SAGE) I (McCormick et al., 1979). SAM II was a one channel instrument which took measurements at high-latitude regions (between 64 and 86° N) for about 12 years between 1979 and 1991. SAGE I was a four channel sun spectrometer taking measurements on a near-global extent (between 80° N and 80° S) between 1979 and 1981. Its successor, SAGE II (McCormick, 1987), was upgraded to seven spectral channels (four of which are suitable for aerosol measurements) and provides the longest continual record of aerosol spectral measurements to date: it operated between 1984 and 2005 for 21 years.

For a volcanic aerosol laden stratosphere, current estimates of aerosol surface area density retrieved from SAGE II measurements are observed to agree well with those inferred from size distributions fit to in situ measurements (Thomason et al., 1997). In contrast, under background aerosol conditions, the retrieved surface area estimates tend to be 40% smaller than those derived from the corresponding in situ data (Deshler et al., 2003; Reeves et al., 2008). Discrepancies have also been observed between SAGE II estimates and in situ measurements of number densities and median particle radii (Bingen et al., 2004a,b). These and other observations gathered in a recent assessment of stratospheric aerosol properties lead to the conclusion that "significant questions remain regarding the ability to characterize stratospheric aerosol during volcanically quiescent periods, particularly in the lower stratosphere" (Thomason and Peter, 2006). A good knowledge of these aerosol properties at the natural background level is, however, an important reference base on which trends can be estimated and perturbations of the climate system can be quantified.

The difficulty associated with retrieving aerosol properties from SAGE II measurements in the volcanically unperturbed stratosphere has to do with the small sizes of background aerosol particles. Median radii are typically between 0.01 and 0.2 µm. One problem is that their contribution to the measured optical extinction is often of the same order of magnitude as the experimental uncertainty. To illustrate this, Table 1 presents the fractional contributions by all particles smaller than 0.1 µm to the total SAGE II spectral extinction, for three different size distributions. They are observed to be similar in magnitude to the listed experimental spectral uncertainty levels. Table 2 lists the associated fractional particle number, surface area and volume. These numbers demonstrate that for two of the three example size distributions the great majority of all particles are smaller than 0.1 µm. Moreover, volume density depends less on the small particles than surface area density.

In addition to the low sensitivity problem, particles that are much smaller than the measurement wavelength are hard or even impossible to discriminate because of fundamental limitations of the scattering theory in the Rayleigh limit (Heintzenberg et al., 1981). The accurate determination of the

particle size distribution parameters and associated integrated aerosol properties depends, however, on all particles including the smallest. This means, that accurate aerosol property estimates can only be obtained by combining the measurements with additional prior information about those particles in the "blind spot" of the experiment.

In response to this need for improved estimates of aerosol properties under background conditions, a new aerosol retrieval model was developed, that uses the Optimal Estimation approach to combine space based measurements of aerosol extinction with prior knowledge about background monomodal size distributions. This way, even the smallest and practically invisible particles are considered in the retrieval process. Section 2 introduces the mathematical description of the aerosol microphysical properties, the basic radiative transfer equations, the SAGE II satellite experiment, and the current SAGE II retrieval method. In Section 3 the new OE retrieval algorithm and the Bayesian approach, which it is based upon, are described. In Section 4 the new OE estimation retrieval algorithm is assessed based on synthetic aerosol extinction data. The a priori data set is described, the retrieved results are presented, and the retrieved as well as additional uncertainties are assessed in a comprehensive error analysis. In Section 5 the new algorithm is applied to near-global SAGE II satellite measurements. The results are presented and discussed in the light of current estimates of aerosol properties retrieved (from the same extinction data but) using different retrieval approaches. Section 6 closes with a summary of the main results and conclusions.

2 Aerosol properties and measurements

The size spectrum of stratospheric aerosol is generally continuous and may range from only a few nanometres up to about 10 micrometres. The most widely used size distribution model for stratospheric aerosols is the differential lognormal expression, given by

$$\frac{dN(r)}{dr} = \sum_i \frac{N_i}{\sqrt{2\pi}\,S_i} \cdot \frac{1}{r} \cdot \exp\left[-\frac{1}{2}\frac{(\ln r - \ln R_i)^2}{S_i^2}\right] \tag{1}$$

where N_i is the total number of particles per unit volume of air, R_i is the median particle radius, and S_i is the half width or standard deviation of mode i. (S is the equivalent of $\ln\sigma$, which is sometimes used in the literature). Monomodal distributions have only one mode, whereas multimodal particle size distributions can be described by a superposition of several modes. $dN/d\ln r$ is the number of particles per unit volume of air in a radius interval between r and $r + dr$. The total number of particles can be calculated by summation over all particle radii and is usually given per cm^3.

The non-volcanic stratospheric background aerosol is usually well described by a monomodal size distribution, although balloon borne in situ measurements indicate that a second mode of larger but less abundant particles can coexist (Deshler, 2008).

From the particle size distribution the associated surface area density and volume density can be derived

$$A = \int_0^\infty 4\pi r^2 \cdot \frac{dN(r)}{dr}\, dr \;=\; 4\pi N R^2 \cdot \exp\left[2S^2\right] \tag{2}$$

$$V = \int_0^\infty \frac{4}{3}\pi r^3 \cdot \frac{dN(r)}{dr}\, dr \;=\; \frac{4}{3}\pi N R^3 \cdot \exp\left[\frac{9}{2}\, S^2\right] \tag{3}$$

where A is usually given in µm^2 per cm^3 and V in µm^3 per cm^3. The effective radius or area-weighted mean radius is given by

$$R_{\text{eff}} = \frac{3V}{A} \;=\; R \cdot \exp\left[\frac{5}{2} S^2\right]. \tag{4}$$

The presence of atmospheric aerosols can be detected based on their effect on other processes in the atmosphere, for instance on the propagation of sunlight. The intensity, I, of electromagnetic radiation transmitted through an inhomogeneous medium is observed to decrease exponentially with increasing distance, s, as described by the Beer-Lambert law:

$$I = I_0 \exp\left[-\beta^{\text{ext}} \cdot s\right], \tag{5}$$

where I_0 is the initial intensity, and β^{ext} the volume extinction coefficient at a particular wavelength. The extinction properties of a medium depend on the efficiency with which light is removed from the beam by absorption and scattering. The volume extinction coefficient can be thought of as the cross-sectional area per unit volume with which the ray interacts. It is the sum of all particle cross-sections multiplied by the extinction efficiency Q^{ext}

$$\beta^{\text{ext}}(\lambda) = \pi \int_0^\infty r^2 \cdot Q^{\text{ext}} \cdot \frac{dN(r)}{dr} dr. \tag{6}$$

The extinction coefficient is conventionally given in $\mu\text{m}^2\text{cm}^{-3}$ or km^{-1} and hereafter just called "extinction". The extinction efficiency Q^{ext} is a function of particle size, of the wavelength of the incident light, and of the refractive index of the substance. As tiny sulphuric acid particles can be assumed to be spherical (Torres et al., 1998) and homogeneous, the extinction coefficient can be calculated using Mie's theory of light extinction (Mie, 1908). The Mie scattering code used in this study originates from the work of Grainger (1990) and can be downloaded from www.atm.ox.ac.uk/code/mie.

The refractive index of sulphuric acid droplets at 1.06 µm ranges between 1.394 and 1.444 for ambient conditions typically found in the lower stratosphere, that is temperatures between 195 K and 240 K, water vapour pressures of $1 \cdot 10^{-4}$ to $8 \cdot 10^{-4}$ hPa, and associated acidities between 35 and 85% by weight H_2SO_4 (Steele et al., 1999). The imaginary part of the refractive index (describing the absorption) is very close to zero and hence extinction is equivalent to scattering.

In this study refractive indices were calculated using a model by Semmler et al. (2003) which is based on laboratory measurements of the densities and refractive indices of binary or ternary

H_2SO_4, and/or $(NH_4)_2SO_4$ and water solutions. The model applies the Lorentz-Lorenz relationship to determine the refractive index at a certain temperature from the refractive index at a reference temperature. The aerosol acidity was determined with the help of temperature and pressure observations (from the National Meteorological Center, NMC) and observed humidity data (SAGE II) and by linearly interpolating between tabulated values from Steele and Hamill (1981) with extensions from Russell and Hamill (1984).

The SAGE II instrument is a seven-channel sun photometer and measures changes in received sunlight as the Sun rises or sets as seen from the spacecraft (solar occultation). A typical SAGE II slant path length is 200 km long for a 1-km thick shell at a tangent height of about 20 km. The optical data are recorded at a series of discrete altitudes (tangent heights) so that vertical distributions of ozone, nitrogen dioxide, water vapour concentration, and aerosol extinction (per km) can be determined. Each day, SAGE II measures approximately 15 sunrise and 15 sunset events, equally spaced in longitude along two latitude belts between 80° N and 80° S. Extremes of latitudes are covered every 4 to 5 weeks. The four wavelengths used for aerosol retrieval are 1.02, 0.525, 0.452, and 0.386 µm. The inversion algorithm is described by Chu et al. (1989). For a description of the optical assembly and operation of the SAGE II instrument the interested reader is referred to McCormick (1987) and McMaster (1986). The SAGE II aerosol extinction data used in this study are a subset of the version 6.1 data made available to the public by the NASA Langley Research Center (LaRC, Hampton, VA, USA).

The operational algorithm used by the NASA LaRC to retrieve integrated aerosol properties from SAGE II aerosol extinction is based on the Principal Component Analysis (PCA) method described by Thomason et al. (1997) and Steele et al. (1999). In the PCA approach, the kernel function in the aerosol extinction equation (Eq. 6) is expanded in terms of a set of orthogonal basis functions. Integral properties such as surface area density and volume density can then be evaluated from a linear combination of the spectral extinction measurements $\beta(\lambda_i)$ multiplied by a factor which is dependent on particle composition (through the aerosol refractive index), on the integration limits employed in the calculation of the eigenvectors and eigenvalues of the covariance matrix, and on the number of principal components retained. The propagation of experimental error can be reduced by narrowing the integration interval and by limiting the number of principal components. This introduces a systematic bias error (Steele et al., 1999).

Operationally, the PCA approach has been modified to move the surface area density derivation dependence toward the 525 and 1020 nm channels, which are more reliable than the short wavelength channels (Thomason et al., 2008). In addition, the relationship for surface area density (SAD) has been simplified for implementation in the operational software using an empirical fit based on the 525 to 1020 nm extinction ratio, r, and the absolute 1020-nm aerosol extinction, k_{1020} (in units of

km^{-1}), that captures approximately 90% of the variance of the original:

$$\mathrm{SAD} = k_{1020} \left(\frac{1854.97 + 90.137\, r + 66,97\, r^2}{1. - 0.1745\, r + 0.00858\, r^2} \right). \quad (7)$$

Observations show that during low aerosol loading periods the operational SAGE II retrieval algorithm tends to underestimate surface area densities derived from in situ data measured by optical particle counters (e.g. Deshler et al., 2003; Thomason and Peter, 2006; Reeves et al., 2008). In a recent sensitivity study Thomason and Peter (2006) found that during background periods the surface area density operational product has an uncertainty of at least a factor of 2. They ascribe this uncertainty to the lack of sensitivity to particles with radii less than 100 nm, the same conclusion arrived at by Deshler et al. (2003).

3 Optimal Estimation retrieval algorithm

In atmospheric remote sensing, the common problem of inverting a set of measured radiances to determine aspects of the atmospheric state (e.g. temperature profile, trace gas mixing ratio profiles, aerosol properties) is often ill-conditioned, meaning that no unique solution exists. Thus additional information of some type is usually required to constrain the retrieval to fall within physically reasonable limits. The new aerosol retrieval algorithm presented here seeks the maximum a posteriori (MAP) solution, which is a specific type of Optimal Estimation (OE) technique (Rodgers, 2000). The general strategy of the OE approach is to seek the solution which is most statistically consistent with both the measured radiances (aerosol extinction) and the typical background aerosol size distributions as represented by the a priori.

Because of the ill-posed problem of retrieving three variables (monomodal size distribution parameters) from Equations (1) and (6), and because of experimental error, a point in state space (particle size distribution) will map into a region of measurement space (spectral aerosol extinction). Conversely, a measurement could be the results of a mapping from anywhere in a region of state space, described by some probability density function, rather than from a single point. The OE retrieval approach is based on Bayesian statistics, which provide a formalism (Bayes' theorem) that translates uncertainty in measurement space into uncertainty in state space. Bayes' Theorem relates a set of measurements, $\boldsymbol{y}$, to the a priori knowledge about the required state, described by a vector $\boldsymbol{x}$. If the a priori, consisting of a mean state and covariance matrix, describes the statistical behaviour of the state vector, Bayes' Theorem allows us to obtain the posterior probability density function (pdf) of a retrieved solution state by updating the prior pdf of the state with the conditional pdf of a measurement:

$$P(\boldsymbol{x}|\boldsymbol{y}) = \frac{P(\boldsymbol{x})}{P(\boldsymbol{y})} P(\boldsymbol{y}|\boldsymbol{x}), \text{where} \quad (8)$$

$P(\boldsymbol{x}|\boldsymbol{y})$ is the posterior conditional pdf of $\boldsymbol{x}$ which describes the probability that the state lies in the interval $(\boldsymbol{x}, \boldsymbol{x} + \boldsymbol{dx})$ when $\boldsymbol{y}$ has a given value; it is the MAP solution.

$P(\boldsymbol{x})$ is the prior pdf of the state $\boldsymbol{x}$ expressing quantitatively our knowledge of $\boldsymbol{x}$ before a measurement is taken.

$P(\boldsymbol{y}|\boldsymbol{x})$ is the conditional pdf of a measurement $\boldsymbol{y}$, which describes the probability that the measurement vector lies in the interval $(\boldsymbol{y}, \boldsymbol{y} + \boldsymbol{dy})$ given a certain state $\boldsymbol{x}$.

$P(\boldsymbol{y})$ describes the knowledge about the measurement before it is taken which is in practice only a normalizing factor (Rodgers, 2000).

This means that all possible states that are consistent with the measured information can be identified and characterized by probability density functions if the following information is given: (a) any prior information about the unknown state, (b) a measurement together with a description of its error statistics, and (c) a forward model. The most likely value of each solution pdf (one for each size distribution parameter) is taken to be "the" Optimal Estimation solution and the width of each solution pdf is the associated (one-sigma) uncertainty. The particular advantage of this approach to the aerosol retrieval problem is that by considering all possible monomodal lognormal size distribution parameters and by weighting them according to their natural probability of occurrence (in the form of pdfs), the Bayesian solution includes also the smallest and effectively invisible aerosol particles. The size discrimination problem of small particles in the Rayleigh limit of scattering is alleviated by prescribing a lognormal size distribution shape.

With the help of Bayes' Theorem and the general expression of the probability function of a vector $\boldsymbol{y}$, the following expression for the general form of the Bayesian solution can be derived (see Rodgers, 2000):

$$-2\ln P(\boldsymbol{x}|\boldsymbol{y}) = [\boldsymbol{y} - F(\boldsymbol{x})]^{\mathrm{T}}\mathbf{S}_{\epsilon}{}^{-1}[\boldsymbol{y} - F(\boldsymbol{x})] + [\boldsymbol{x} - \boldsymbol{x_a}]^{\mathrm{T}}\mathbf{S_a}{}^{-1}[\boldsymbol{x} - \boldsymbol{x_a}] + c, \quad (9)$$

where $F(\boldsymbol{x})$ is the forward model expressing spectral aerosol extinction in terms of the size distribution parameters, $\mathbf{S}_{\epsilon}$ is the measurement error covariance matrix, $\boldsymbol{x_a}$ and $\mathbf{S_a}$ are the a priori mean state and covariance matrix, and c is a constant. In this form it can be seen that the MAP retrieval solution combines to independent estimates of the same vector quantity (i.e. the state vector determined solely from the measurement vector $\boldsymbol{y}$ and a virtual measurement represented by the a priori state vector $\boldsymbol{x_a}$) inversely weighted by their respective covariances. However, if the a priori pdf is appropriate, the solutions will be biased only within experimental uncertainty (Rodgers, 2000). The quadratic form in $\boldsymbol{x}$ implies that it must be possible to express $\ln P(\boldsymbol{x}|\boldsymbol{y})$ as a function of a new state $\hat{\boldsymbol{x}}$ (retrieval solution) and an associated error covariance $\hat{\mathbf{S}}$:

$$-2\ln P(\boldsymbol{x}|\boldsymbol{y}) = [\boldsymbol{x} - \hat{\boldsymbol{x}}]^{\mathrm{T}}\hat{\mathbf{S}}^{-1}[\boldsymbol{x} - \hat{\boldsymbol{x}}]. \quad (10)$$

An explicit expression for $\hat{\mathbf{S}}$ can be derived when assuming that within a small particle size range the forward model can be approximated by a linearised forward model of the form $F(\boldsymbol{x}) = \nabla_x F(\boldsymbol{x_0})(\boldsymbol{x} - \boldsymbol{x_0}) = \boldsymbol{y_0} + \mathbf{K}_0\ (\boldsymbol{x} - \boldsymbol{x_0})$, where $\boldsymbol{x_0}$ is an arbitrary linearisation point and

$\mathbf{K}_0$ is the Jacobian matrix of derivatives at $\boldsymbol{x_0}$. This approach is appropriate as the problem is no more than moderately non-linear, meaning that the difference between the forward model and a linearised version of the forward model remains within the solution error covariance. Equating terms that are quadratic in $\boldsymbol{x}$ then leads to an expression for the inverse covariance matrix

$$\hat{\mathbf{S}}^{-\mathbf{1}} = \mathbf{K}^{\mathbf{T}}\mathbf{S}_{\epsilon}^{-\mathbf{1}}\mathbf{K} + \mathbf{S}_{\mathbf{a}}^{-\mathbf{1}}, \tag{11}$$

where $\mathbf{K}$ is the Jacobian or weighting function matrix containing the partial derivative of $F(\boldsymbol{x})$ with respect to the state vector elements.

The expected MAP retrieval state is situated where the posterior pdf takes a maximum. This is equivalent to finding the minimum on a multidimensional surface which is given by the right hand side of Eq. (9). This leads to the following implicit expression for $\hat{\mathbf{x}}$

$$-\hat{\mathbf{K}}^{\mathbf{T}}\mathbf{S}_{\epsilon}^{-\mathbf{1}}[\boldsymbol{y} - \hat{F}] + \mathbf{S}_{\mathbf{a}}^{-\mathbf{1}}[\hat{\boldsymbol{x}} - \boldsymbol{x_a}] = 0, \tag{12}$$

where $\hat{\mathbf{K}}$ is the Jacobian matrix of derivatives at the solution state. Application of the Levenberg-Marquardt root-finding method (Press et al., 1992) and dropping the second derivative of the forward model leads to the following iterative equation for the solution state

$$\begin{aligned}\boldsymbol{x_{i+1}} = \boldsymbol{x_i} + (\mathbf{S}_{\mathbf{a}}^{-\mathbf{1}} + \mathbf{K}_{\mathbf{i}}^{\mathbf{T}}\mathbf{S}_{\epsilon}^{-\mathbf{1}}\mathbf{K}_{\mathbf{i}} + \gamma\mathbf{S}_{\mathbf{a}}^{-\mathbf{1}})^{-1} \cdot \\ (\mathbf{K}_{\mathbf{i}}^{\mathbf{T}}\mathbf{S}_{\epsilon}^{-\mathbf{1}}[\boldsymbol{y} - F(\boldsymbol{x_i})] - \mathbf{S}_{\mathbf{a}}^{-\mathbf{1}}[\boldsymbol{x_i} - \boldsymbol{x_a}]),\end{aligned} \tag{13}$$

where γ is chosen at each step to minimise the right hand side of Eq. (9) and such that the new value of $\boldsymbol{x}$ remains within the linear range of the previous estimate.

In our aerosol retrieval model the measurement vector, $\boldsymbol{y}$, consists of a set of four volume extinction coefficients, one for each of the four SAGE II aerosol spectral channels. The state vector is a three element vector containing the natural logarithms of the three monomodal size distribution parameters, $\boldsymbol{x} = \ln[N, R, S]$. This form is particularly suitable because in log-space (a) the size distribution parameters are approximately normally distributed, (b) the different orders of magnitude of N (1–100 particles per cm^3), R (0.001–1.0 µm) and S (0.1–1 in log radius) are merged to a similar scale, and (c) the solution space is positive definite and hence naturally constrained to physically sensible solutions.

The forward model $F_\lambda(\boldsymbol{x})$ expresses the aerosol extinction at a particular wavelength λ in terms of the monomodal log-normal size distribution parameters

$$F_\lambda(\boldsymbol{x}) = \sum_{\ln r_a}^{\ln r_b} \pi r^2 \cdot Q^{\mathrm{ext}}(r, \lambda, \mathrm{RI}) \cdot \frac{\mathrm{dN(r)}}{\mathrm{d}\ln \mathrm{r}} \Delta \ln \mathrm{r}, \tag{14}$$

where r is the particle radius at which the function is evaluated, r_a and r_b are finite integration limits between which the integrand is non-negligible, $\Delta \ln r$ is the width of the particle size interval, and RI is the aerosol refractive index at wavelength λ.

Each retrieval process is initialised with a first guess of the aerosol state. The first retrieval process starts with the a priori mean state as first guess. As usually subsequent measurements were taken at adjacent heights, aerosol properties retrieved at height k are used as a first guess state at height $k+1$. In case a retrieval process does not converge, the adjacent measurements are initialised with the a priori mean state.

Whether or not a retrieval process has converged to sufficient precision is decided based on the size and rate of change of the retrieval cost (right hand side of Eq. 9), on the differences (between two consecutive iterations) in the retrieved signal and in the retrieved state vector elements, and on the number of iterations performed. The computational efficiency and accuracy of the forward model are optimized by adapting the number of grid points to the smoothness of the integrand and by individually estimating suitable integration limits for each measurement vector. As a result solutions are found quickly and mostly obtained in less than five iterations.

4 Model validation

4.1 A priori data

In principle, the a priori represents the expected statistical behaviour (both in terms of the mean state and variability) of the state vector. Prior information about aerosol particle size distributions can be gained from in situ balloon borne size resolved concentration measurements (Deshler et al., 2003). The size distributions used in this study were measured between May 1991 and October 1997 by the University of Wyoming at Laramie (41° N, 105° W) at altitudes between 20 and 35 km. Although the majority of measurements taken during this period indicate bimodal size distributions that were at least partly influenced by the eruption of Mt. Pinatubo (June 1991, 15° N), only monomodal background data were selected. These 264 monomodal aerosols size distributions have median particle radii between 0.02 and 0.2 µm and are clearly non-volcanic. Given the fact that comparable in situ measurements at other latitudes are rather scarce to date, the Laramie record currently represents our best knowledge of aerosol properties under background conditions.

Probability density functions (characterized by a mean and covariance matrix) of number density, median radius and distribution width were generated based on these measurements, which were collected at different altitudes and times of the year and are therefore representative of a range of temperatures and acidities. It will be shown that good retrieval results are achieved using the a priori knowledge in this form. The limitations of this choice are discussed in Section 4.3.

4.2 Retrieval from synthetic extinction

To assess the performance of the new retrieval algorithm synthetic extinction coefficients (at 0.385, 0.452, 0.525 and 1.020 µm) were calculated for a 75% (by weight) sulphuric acid solution at 300 K (refractive indices by Palmer and Williams, 1975) and based on the monomodal a priori size dis-

tributions described in Sect. 4.1. By adding two different noise components, two test beds were generated: (a) the Minimum Noise Scenario (minNS) is characterised by a 1% Gaussian distributed random noise component added onto each of the four spectral extinction data; (b) the Maximum Noise Scenario (maxNS) is characterised by [60, 45, 30, 25]% Gaussian distributed random noise on the respective spectral channels [0.385, 0.452, 0.525, 1.020] µm. These noise levels describe the range of typical SAGE II extinction uncertainties, with the majority of all experimental uncertainties lying between the two extremes.

As these test data cover the entire range of monomodal size distributions as measured in situ (41° N) at different altitudes and times of the year, the two test beds can be considered comprehensive and suitable to test the performance of the OE retrieval algorithm for monomodal background aerosol particles. The a priori pdfs are perfect in the sense that they describe exactly the same ensemble of size distributions that we expect to retrieve in the case of a perfectly successful retrieval model. A bias due to the a priori and the ensemble of test aerosols size distribution being identical is not given because only one set of extinction measurements describing one of the entire ensemble of a priori distributions is analysed at a time.

The OE retrieval was applied to all test bed data. To discard spurious retrieval solutions an ad hoc quality filter was developed based on several retrieval diagnostics. This filter achieves a good balance between maximizing the correlation between the retrieved and the correct solutions and minimizing data loss through rejection. In both noise scenarios approximately 88% of all retrieved solutions pass the screening.

Figure 1 presents all retrieved size distribution parameters in the form of histograms. In can be observed that all three variables are symmetrically distributed about the a priori mean and in fact with a frequency distribution very similar to the a priori data ensemble (not shown). The same is true for for the derived integrated properties A, V, R_{eff} presented in Figure 2.

Figure 3 (minNS) and Figure 4 (maxNS) display the retrieved aerosol properties versus the true values. The associated linear correlation coefficients are listed in Table 3. Presented in this form it becomes obvious that the retrieved and the true values are well correlated and that the best agreement between the true and the retrieved solutions is found in surface area density, volume density and effective radius. This observation can be explained by the fact that A, V, and R_{eff} are integrated quantities, whereas number density, median radius and distribution width are functions in the integral (Eq. 2 and Eq. 3 with $N(r)$ given by Eq. 1). Fluctuations and uncertainties on the size distribution parameters are smoothed out during integration such that A, V, and R_{eff} have a higher stability than N, R, and S from which they were derived. Conversely, small fluctuations and uncertainties of the extinction (Eq. 6), which is an integrated quantity, give rise to a highly amplified fluctuation of the functions in the integral, i.e. on N, R and S. In addition, the integrated aerosol properties are less sensitive to the small and hard to retrieve particles than the size distribution parameters which directly depend on all particles (Tab. 1 and Tab. 2). Nevertheless, the median radius (Fig. 3.b

and Fig. 4.b) can be observed to be fairly accurately retrieved at values greater than approximately 0.02 µm ($\log_{10}(-1.7)$), even in the case of large extinction uncertainty. As might be expected, less experimental noise allows for more accurate retrieval solutions which results in higher correlation coefficients. Table 4 lists the ensemble mean errors of all six variables in both noise scenarios. A comparison with the initial uncertainties ($\sigma_N = 93\%$, $\sigma_R = 61\%$ and $\sigma_S = 31\%$ from the a priori variances) shows that, as might be expected, the latter were clearly reduced by updating the a priori pdf with the measurements (using Bayes' Theorem). The retrieved uncertainties are generally and naturally larger in the case of large noise (Fig. 4) than in the case of little extinction error (Fig. 3). The observation that the uncertainty in N is highest confirms that number density is harder to retrieve than the other five aerosol properties.

4.3 Error Analysis

The retrieved uncertainties result from the propagation of measurement error and from the influence of the a priori constraint (Eq. 11). In the case of synthetic data the retrieved errors can be directly compared with the true error, i.e. the difference between the retrieved and the correct value. This comparison indicates that the retrieved errors are generally a good representation of the true errors although slightly overestimating the true errors in the maximum noise scenario (Wurl, 2008).

In the case of measured data additional uncertainties have to be considered. There could be contributions from forward model error and from forward model parameter errors, an a priori bias due to a potentially inappropriate a priori constraint, and a bias due to analysing bimodal aerosol data with a monomodal retrieval model.

The forward model error is the difference between the exact physics and the mathematical model. There are basically three sources of uncertainty: (a) deviations from Mie theory, (b) deviations from the lognormal particle size distribution model, and (c) numerical errors. Since the tiny sulphuric acid and water droplets of background aerosols found at temperatures above the frost point (Rosen, 1971; Steele and Hamill, 1981) are expected to be spherical and homogeneous, deviations from Mie theory are assumed to be small. Numerical forward model errors arising from discretisation of the model equations and from truncation of the integration integral are estimated to be smaller than 1% in aerosol extinction (Wurl, 2008). This is clearly smaller than the 10–60% measurement noise typically observed at 0.368 µm, but not necessarily negligible compared to the 1–10% measurement noise typically observed at 1.020 µm. As size resolved concentration measurements appear to be well approximated by lognormal distributions (Deshler et al., 2003), uncertainties arising from any discrepancies to the true size distributions are expected to be small compared to the experimental uncertainty.

The forward model parameter error arises from uncertainties in parameters that are not part of the state vector but nevertheless influence the measurements. In this retrieval model these are the atmospheric temperature and water vapour partial pressure, sulphuric acid concentration and refrac-

tive index. A common approach to estimate the forward model parameter error is to use best-guess values and a random deviation of the "true" atmosphere about this guess. When size distribution parameters were retrieved from spectral extinction data simulated for a typical background aerosol (N=4.7 cm^{-3}, R=0.04 µm and S = 0.48) at two reference states (220 K / 70%; 200 K / 65%) and two fluctuation scenarios ($\pm$1 K / $\pm$1%; $\pm$5 K / $\pm$5%), the forward model error was found to be always less than 3% in N, R, and S. This is generally over an order of magnitude smaller than the retrieved uncertainties (Table 4) which indicates that the forward model parameter error tends to be negligible compared to the measurement uncertainties mapped into solution space.

The purpose of the a priori pdf is to add to the information contained in the measurements by describing the solution space as comprehensively as possible.

As the loading of aerosol varies with height and latitude as the tropopause height changes, as well as with time (e.g. with season of the year or with the phase of the quasi-biannial oscillation, Trepte and Hitchman (1992)) the ideal a priori information would be a function of latitude, altitude, and time. However, given the paucity of aerosol measurements (other than SAGE) it seems more reasonable to use a broad a priori pdf that captures the variation with height and latitude. Firstly, as the a priori becomes more specific (either spatially or temporally), the a priori variances and covariances would be expected to decrease. In the maximum a posteriori technique, this will tend to decrease the relative weight of the measured extinction in the aerosol retrieval and thereby increase he relative weight of the a priori mean state. And secondly, our experience of satellite retrievals suggests that using spatially-varying a priori may produce spurious features in the retrieved fields (Deeter et al., 2003). Neither of these effects is desirable at present, as they both would complicate interpretation of the retrieval results.

The Wyoming in situ record (Sect. 4.1) comprises aerosols measured at different altitudes and different times of the year. It is therefore representative of a range of different temperatures and acidities. As these were, however, all measured at mid-latitudes (41° N), they may not be entirely representative of all aerosols that may occur at other latitudes. A comparison with a series of in situ measurements taken at Lauder, New Zealand (45° S, 1991–2001) shows that these southern mid-latitude aerosols are very similar to the Laramie (41° N) time series (Deshler et al., 2003). A bias due to the a priori data being potentially unrepresentative of some aerosols that may occur at other latitudes can only be estimated when new measurements become available in the future.

The results obtained with the height- and time-independent comprehensive a priori (Sect. 4.1) were shown to be fairly accurate even in the case of large measurement uncertainty (Sect. 4.2).

4.4 Bimodal aerosols

Another aspect that introduces uncertainty is whether the use of a monomodal retrieval model is appropriate given that size resolved particle concentrations measured in the volcanically unperturbed stratosphere are often better described by bimodal than by monomodal particle size distributions

(Deshler et al., 2003). A comparison (not shown) between monomodal and bimodal data measured in situ between 1997 and 2001 indicates that monomodal aerosols are very similar to those described by the smaller mode of the bimodal distributions, with typical median radii between 0.01 and 0.2 µm. The second mode tends to be small containing only very few, but larger particles with median radii between 0.2 and 0.8 µm.

In order to assess the capability of the monomodal OE retrieval model to accurately determine the properties of small-mode-dominant bimodal aerosols, synthetic extinction data were generated in the same way as for the two monomodal test beds (Sect. 4.2), but based on 244 bimodal background aerosol size distributions measured in situ near 41° N between January 1997 and May 2002 at altitudes between 20 and 35 km (Deshler et al., 2003). A comparison between these spectral extinction data with those generated from monomodal background aerosol (Sect. 4.2) shows that both cover basically the same range and are therefore not distinguishable prior to the retrieval analysis. This agrees with results by Steele and Turco (1997) who found that it is possible for bimodal size distributions to account for extinctions generated from monomodal distributions and vice versa. The OE retrieval algorithm was then applied to the synthetic extinction data to retrieve monomodal size distribution parameters. About 91% of all data analysed (223 out of 244) passed the ad hoc quality filter and are presented below. Figure 5 displays frequency distributions of the size distribution parameters retrieved in the presence of large extinction uncertainty (maxNS). It can be observed that the peak values of the N, R and S retrieved from bimodal distributions are larger than the a priori mean. Compared to the those values retrieved from monomodal aerosol data (Fig. 1), only a few N and R are smaller than the a priori mean. Nevertheless, all solutions are within the range described by the a priori pdfs. Figure 6 shows that a similar shift to larger values can be observed in the derived integrated properties (compared with Fig. 2). A comparison with histograms of the correct aerosol properties, separated into mode 1 and mode 2 (not presented), shows that the retrieved monomodal R, A and V are very similar to the first mode of small-mode-dominant bimodal distributions. This indicates that the minority of large particles play a minor role in determining median radius, surface area and volume density, which can hence be expected to be well retrieved even assuming a monomodal model.

Figure 7 shows a comparison between the retrieved (monomodal) integrated aerosol properties A, V, and R_{eff} and the correct bimodal solutions. The retrieved surface area densities (Fig. 7.a) are observed to match the true (bimodal) solutions well except at values greater than approximately 1.0 µm^{2}cm^{-3}, where retrieved (monomodal) A tend to underestimate the correct (bimodal) solutions. This bias probably explains why the linear correlation coefficient, 0.87, is noticeably smaller than 0.94 in the case of monomodal aerosol (Tab. 3). The retrieved and the correct bimodal volume densities (Fig. 7.b) have a high linear correlation coefficient, 0.96, which is only slightly (but significantly at p=0.0001%) smaller than that in the case of monomodal aerosol (0.98, Tab. 3). A slight tendency to underestimate the true volume densities is observed at values larger than 0.05 µm^{3}cm^{-3}

($\log_{10}(-1.3)$). The comparatively low correlation coefficient observed in R_{eff}, 0.38 (Fig. 7.c), can be explained by the effective radius (Eq. 4) being sensitive to errors in A and V. The monomodal retrieval model tends to overestimate the correct R_{eff}. Nevertheless, the retrieved solutions generally agree with the correct values within the retrieved uncertainties. The retrieved uncertainties in A and V are equally realistic (Wurl, 2008), except at surface area densities exceeding the $1.0\,\mu m^2 cm^{-3}$ threshold where the true error is underestimated.

Bauman et al. (2003a), who use a multi-wavelength look-up table (LUT) algorithm as a basis for aerosol retrievals, have done a similar analysis to study the effect of assuming a monomodal size distribution, when the actual distribution is bimodal. They tested the bias with synthetic input spectra (with no uncertainty from measurement error or spatiotemporal variability) and found that the retrieved surface area and volume densities tend to underestimate the correct bimodal values, whereas the retrieved effective radii are larger than the correct values in the case of small-mode-dominant bimodal distributions. In principle, the OE results agree with the LUT findings. However, a noticeable bias is only observed at surface area and volume densities greater than $1.0\,\mu m^2 cm^{-3}$ and $0.05\,\mu m^3 cm^{-3}$, respectively.

In summary, the above assessment of the retrieved and potential additional uncertainties has shown: The retrieved errors are generally a realistic estimate of the true errors, except at surface area densities larger than $1.0\,\mu m^2 cm^{-3}$ where the retrieved uncertainty estimates tend to underestimate the true errors. A bias due the mid-latitude a priori data being potentially unrepresentative of typical aerosols at other latitudes can only be quantified when new in situ measurements become available in the future.

5 Application to measured data

5.1 Retrieval from SAGE II measurements

The new Optimal Estimation aerosol retrieval algorithm was then applied to SAGE II satellite measurements recorded in December 1999. This data consists of approximately 19 700 sets of spectral aerosol extinction data measured between 70° S and 40° N in the lower stratosphere at altitudes between 12 and 35 km. As the year 1999 is part of the longest volcanically quiescent period in the SAGE II record which began around 1997 (Deshler et al., 2006), the aerosols are assumed to consist of tiny spherical sulphuric acid particles. Measured temperature, pressure and humidity data (associated with the extinction measurements) are used to calculate the aerosol acidity, which is then used to determine the aerosol refractive index using a model by Semmler et al. (2003). The a priori data is used as described in Sect. 4.1. The OE retrieval algorithm was applied to all measurements with experimental uncertainties smaller than 99%. Nearly all retrieval processes converged to a solution, and those results which passed the ad hoc quality screening (approximately 90%) are presented below.

Figure 8 presents the retrieved size distribution parameters in the form of histograms. It becomes immediately apparent that the number densities, median radii and distribution widths retrieved from SAGE II measurements of aerosol extinction are very similar to those retrieved from synthetic extinction by bimodal background aerosol (Fig. 5). Both data sets have peak frequencies at similar values larger than the a priori mean, and the great majority of all results are observed to be within one standard deviation of the a priori mean. The ensemble mean retrieved linear size distribution parameters and a priori ensemble means are listed in Table 5.

Figure 9 displays frequency distributions of the integrated aerosol properties derived from the retrieved size distribution parameters shown above (Fig. 8). A similar resemblance (as observed in N, R, and S) to those results retrieved from bimodal aerosol data can be detected in surface area density, volume density, and effective radius. The peak frequencies of the SAGE II data are, however, slightly larger than those observed in Figure 5. The ensemble mean retrieved and a priori values are listed in Table 6. The similarity with those aerosol properties retrieved from synthetic extinction by bimodal background aerosols (Sect. 4.3) suggests that the aerosols measured by SAGE II could have been predominantly bimodal. This means that the retrieved number densities, distribution widths and effective particle radii may be less accurate, and surface areas greater than 1.0 $\mu m^2 cm^{-3}$ and volume densities greater than 0.05 $\mu m^3 cm^{-3}$ could be underestimated due to the monomodal forward model.

Figure 10 presents the retrieved uncertainties σ_N, σ_R and σ_S. A comparison with the model validation results (see Table 4) shows that, as might expected, the OE uncertainties retrieved from SAGE II measurements are larger than those in the minimunm noise scenario and smaller than those achieved in the maximum noise scenario. The associated uncertainties in the integrated properties, σ_A, σ_V, σ_{Reff}, are presented in Figure 11. The ensemble mean uncertainties of all retrieved aerosol properties are listed in Table 5 and Table 6.

5.2 Discussion

In order to assess how the new Optimal Estimation algorithm can add to the current knowledge of aerosol microphysical properties in the volcanically unperturbed lower stratosphere, the retrieved results are compared to aerosol properties estimated through different retrieval techniques as well as to correlative in situ data.

The NASA Langley Research Center retrieves surface area density and effective radius from SAGE II aerosol extinction data using the Principal Component Analysis (PCA) technique (Sect. 2). The associated volume densities can be derived using Eq. (4). Figure 12 shows the PCA solutions versus the Optimal Estimation results, all retrieved from the same SAGE II extinction measurements. The correlation coefficients, 0.94 in A, 0.98 in V, and 0.76 in R_{eff}, indicate a good (and highly significant) linear correlation between the two data sets, however, there is a systematic bias. The great majority of all OE surface areas and volumes are larger than the associated PCA values, whereas OE effective radii are smaller than the PCA solutions. Figure 13 presents the relative differences (in %)

between the respective method results,

$$\Delta x = \frac{(x_{\mathrm{PCA}} - x_{\mathrm{OE}})}{x_{\mathrm{OE}}} \cdot 100. \quad (15)$$

The PCA surface area and volume densities are observed to be smaller by respective 20 to 50% and 10 to 40%, whereas the PCA effective radii tend to be 10 to 40% larger than the respective OE values.

Similar biases have previously been observed between PCA retrieval results and in situ data. In particular, Steele et al. (1999) found that retrieved surface areas for background aerosol can be underestimated by up to 50% and volume densities by up to 30% through Principal Component Analysis. Deshler et al. (2003) observed that for background aerosol conditions the SAGE II estimates of surface area density retrieved through Principal Component Analysis are about 40% lower than those calculated from correlative in situ measurements. Reeves et al. (2008) come to similar conclusions based on comparisons of SAGE II estimates with near coincident in situ aircraft measurements of aerosol size distributions. This suggests that the new OE estimates tend to be more realistic and hence improved compared to current estimates of aerosol properties in the volcanically unperturbed lower stratosphere.

To directly compare correlative OE, the PCA and the in situ (Optical Particle Counter, OPC) surface area densities, the SAGE II and the in situ data sets were searched for correlative measurements. In 1999, the University of Wyoming (41° N, 105° W) performed in situ measurements on six dates: March 22, April 20, June 23, July 21, September 16, and December 10. As, however, only two SAGE II measurement events coincide with these dates and location, the time constraint was slightly relaxed to allow for measurements recorded within a few days of the Laramie balloon flights. The four SAGE II measurement events identified this way differ from the two correlative in situ measurement by up to 6 days, 2° in latitudinal and 5° in longitudinal direction. Bearing in mind that the observed differences will result from a combination of differences in the measurement characteristics (different measurement techniques, recording times, location) as well as systematic differences between the OE and PCA retrieval results, the PCA and OE retrieval results are now compared to the correlative in situ data in the form of vertical profiles. The relative difference between any two values at a particular altitude is given in % of the in situ value

$$\Delta x_i = \frac{(\hat{x}_i - x_{i,\mathrm{OPC}})}{x_{i,\mathrm{OPC}}} \cdot 100, \quad (16)$$

and the profile mean difference is the arithmetic mean of all differences (absolute numbers) in the profile. Figure 14 shows a comparison between vertical profiles of surface area density as retrieved from SAGE II using the PCA approach versus the correlative in situ surface area densities of monomodal background aerosol. In June (Fig. 14.a and Fig. 14.c), distinct deviations can be observed below 19 km, where the in situ surface area densities take values of 1.9 $\mu m^2 cm^{-3}$. At these lower altitudes, the PCA retrieval solutions are 30 to 70% smaller than the in situ values (Fig. 14.b

and Fig. 14.d). A comparison with the associated in situ number densities and median radii (not shown) helps to understand the observed differences: the particle radii decrease from 0.06 µm at 19 km to about 0.02 µm at 13 km; simultaneously the number density increases strongly from about 10 to over 100 particles per cm^3 at 13 km (near the tropopause), which explains the observed increase in A toward lower altitudes. In December (Fig. 14.e and Fig. 14.g), the PCA surface area densities are observed to be almost consistently smaller by about 30 to 40% compared to the in situ values (Fig. 14.f and Fig. 14.h).

Figure 15 displays the same comparison for the OE retrieval results. As the OE surface area densities are generally higher than the PCA values shown above, the difference to the a priori values below 19 km (Fig. 15.a and Fig. 15.c) has decreased. In Fig. 15.a the two profiles even agree within the OE uncertainties. Between 20 and 23 km the A_{OE} are observed to be larger than the in situ values. In December (Fig. 15.e and Fig. 15.g), the OE surface area densities are observed to widely agree with the in situ values within the respective uncertainties.

Cross-comparisons between the different retrieval method results shows that the OE profiles (Fig. 15) and the PCA profiles (Fig. 14) of surface area densities are similar in their vertical structure, although the PCA surface area densities are generally smaller than the OE values. The OE and PCA results are observed to converge near 24 km, where the particle sizes are largest (0.08 µm). Above as well as below the monomodal aerosols observed in situ tend to decrease in size. Overall, the profile comparisons suggest that the Optimal Estimation surface area densities tend to match the in situ values better than the Principal Component Analysis solutions.

Bingen et al. (2004a,b) retrieved particle number density and median particle size from SAGE II aerosol extinction measured between 1984 and 2000 using a regularized inversion retrieval technique. Compared to the OE results the particle radii retrieved by Bingen et al. (2004a) are about three times as large. For instance, at an altitude of 17.5 km at mid-latitude (40 to 70° N/S) in 1999, the retrieved radii range between 0.25 and 0.33 µm (NH) or 0.27 and 0.37 µm (SH), whereas the OE results are on the order of 0.08 µm. Simultaneously, the number densities retrieved by Bingen et al. (2004b), which they found to be low compared to coincident in situ Optical Particle Counter measurements (Bingen et al., 2004b), are smaller than the OE number densities. Bingen et al. ascribe their low number densities and overestimated particle sizes to the inability of SAGE II optical measurements to discriminate very thin particles in the Rayleigh limit of scattering. This suggests that the larger OE number densities and smaller OE median radii tend to be more realistic than those presented by Bingen et al. (2004b).

Error estimates associated with the retrieved solutions are ideally a good representation of the difference between the retrieved and the correct solutions. Achieving realistic uncertainty estimates, however, is in practice often difficult, because not all biases can be reliably estimated under certain circumstances. Consequently, some error estimates presented in the literature may represent partial uncertainties only and can therefore not give conclusive evidence of the accuracy of the achieved

results. Nonetheless, uncertainty estimates do give an indication of the quality of the retrieved results provided that the scope of their application (all included aspects and expected additional uncertainties) is taken into account.

Table 7 provides a list of uncertainty estimates associated with aerosol properties all retrieved under non-volcanic conditions but using different retrieval techniques. The "+" indicates that a given value is an estimate of partial errors only and that the total error is expected to be higher due to other disregarded uncertainty components. Generally, it can be observed that in surface area, volume density and effective radius the OE retrieved uncertainty estimates are of a similar size to those values reported in the literature. For the number size distribution parameters there are less values to compare and larger differences between the data sets. In number density, the uncertainties reported by Bingen et al. (2004b) are larger than the OE error estimates, whereas those estimated by Wang et al. (1989) are considerably smaller. The 11% reported by Wang et al. (1989), however, account only for particles greater than 0.15 µm although the great majority of the retrieved OE sizes are smaller than that (Fig. 8). Similarly, uncertainties in median particle radius estimated by Wang et al. (1989) are smaller than those reported by Bingen et al. (2004b) and smaller than those achieved through Optimal Estimation, but their error estimates apply only to radii between 0.1 and 0.7 µm. However, although particles smaller than 0.1 µm may contribute little to the total aerosol extinction, their contribution is important to get accurate estimates of the retrieved aerosol properties (Sect. 1).

The uncertainties in surface area density, volume density, and effective radius reported by Bauman et al. (2003a) describe the retrieval uncertainties after a correction for a bias error due to the assumption of a monomodal size distribution. These values do not take into account contributions resulting from the propagation of measurement uncertainty, which will have to be added on top.

In contrast, the uncertainties retrieved through Optimal Estimation (assessed in Sect. 4.3) were found to be a good description of the true errors (a) in all retrieved size distribution parameters and integrated properties, where the true aerosols are monomodal, and (b) at least for all integrated aerosol properties (except where A is greater than 1.0 $\mu m^2 cm^{-3}$) in the case of bimodal background aerosols. The only uncertainty aspect which cannot be estimated at present is a potential bias due to the Wyoming in situ data being potentially unrepresentative of some aerosols that may occur at other latitudes.

Figure 16 illustrates the locations of SAGE II measurement events in four different seasons in 1999. Figure 17 presents the resulting number of measurements counted into 10° latitude by 1 km altitude grid box boxes. Due to the SAGE II measuring geometry, the great majority of all data measured in December were recorded at northern mid-latitudes, namely near 40° N. This means that the a priori data used in this study would be appropriate at least for the majority of all data presented here. In contrast, most of the September measurements were recorded at higher latitudes, namely near 60° N and S. If the retrieved aerosol properties in September were distinctly different from the December data, this could be an indication that the measured aerosols were not appropriately

represented by the mid-latitude a priori size distributions. In Figure 18 (September data), no great discrepancies to the results retrieved in December (Fig. 8) can, however, be observed. This means that the applicability of the current mid-latitude a priori for aerosols measured at other latitudes in the SAGE record cannot be disproved until new in situ measurements become available.

6 Summary and conclusions

We have introduced a new Optimal Estimation algorithm which retrieves monomodal number size distribution parameters and associated uncertainties from spectral aerosol extinction measured at visible to near infrared wavelengths under non-volcanic conditions. The particular challenge of this ill-posed aerosol retrieval problem arises from the low sensitivity of the available aerosol extinction measurements to particles smaller than 0.1 µm combined with the difficulty of discriminating particle sizes in the Rayleigh limit of Mie scattering. The Optimal Estimation algorithm approaches this problem with the help of Bayes' Theorem, which translates uncertainty in measurement space into uncertainty in state space and identifies the monomodal size distribution parameters which are statistically most consistent with both the satellite-measured multi-wavelength aerosol extinction data and the a priori information. By thus considering all particle sizes and by weighting them according to their natural probability of occurrence, even the smallest and practically invisible particles are considered in the solution process. The size discrimination problem at the small particle end is alleviated by prescribing an analytical lognormal size distribution shape.

The new OE retrieval algorithm was tested on synthetic monomodal and small-mode-dominant bimodal aerosol size distributions and then applied to a large set of spectral SAGE II aerosol extinction data recorded in 1999. The results were compared to other estimates of aerosol properties retrieved from remotely sensed data (using different retrieval approaches) and also to correlative in situ measurements. We found:

- Aerosol properties retrieved from synthetic extinction data are generally well correlated with the true solutions, even in the presence of large extinction uncertainty. The best agreement between the true and the retrieved solutions is found in the integrated properties, namely in surface area density, volume density and effective radius.

- In the case of bimodal aerosols, the retrieved monomodal parameters can be expected to naturally deviate from the correct bimodal values. Nevertheless, the integrated aerosol properties can be accurately retrieved except at surface area densities greater than $1.0\,\mu m^2 cm^{-3}$ and at volume densities greater than $0.05\,\mu m^3 cm^{-3}$, where they tend to underestimate the correct bimodal values.

- The comprehensive (as opposed to height- or time-resolved) a priori probability density functions were found to be appropriate for retrieving aerosol properties from synthetic measure-

ments, even in the case of large extinction uncertainty and in the case of small-mode-dominant bimodal aerosols (with the exceptions named above). A bias due to the Wyoming data being potentially unrepresentative of aerosols at other latitudes cannot be detected in the retrieved results. At present, the mid-latitude in situ measurements provide the best prior estimate we have, and the retrieval results seem to confirm the validity of their use.

– The retrieved uncertainty estimates are of the order of 69% for number concentration, 33% for median radius, 14% for the lognormal distribution width, 23% for surface area density, 12% for volume density, and 13% for effective radius. Compared to retrieval errors reported by other researchers the OE uncertainties are smaller (for number density, median radius and distribution width) or of the same order of magnitude (for surface area density, volume density, and effective radius). While some of the uncertainty estimates provided by other researchers represent partial errors only, the uncertainties retrieved through Optimal Estimation were found to be a good description of the true errors: (a) in all retrieved size distribution parameters and integrated properties, where the true aerosols are monomodal, and (b) at least for all integrated aerosol properties (except where A is greater than 1.0 $\mu m^2 cm^{-3}$) in the case of bimodal background aerosols. Additional error contributions from typical forward model errors and from forward model parameter errors tend to be small compared to the experimental uncertainty. The only uncertainty aspect which cannot be estimated at present (due to a lack of in situ aerosol measurements at other latitudes) is a bias due to the Wyoming in situ data being potentially unrepresentative of some aerosols that may occur at other latitudes.

– A comparison of the OE retrieval results with integrated aerosol properties retrieved from the same SAGE II data set but using the Principal Component Analysis (PCA) approach indicates that the OE surface areas tend to be larger by 20 to 50%, the OE volumes tend to be larger by 10 to 40%, and the OE effective radii tend to be 10 to 40% smaller than the respective PCA values. As PCA surface area densities (retrieved from the same SAGE II measurements) are known to underestimate correlative in situ data by about 40% (Deshler et al., 2003; Reeves et al., 2008) and that the PCA volume densities tend to be low by an estimated 30% (Steele et al., 1999), these observations suggest that the new OE algorithm provides improved aerosol property estimates.

– The OE number densities are larger and the median radii are smaller than the number densities and median radii retrieved by Bingen et al. (2004a) from SAGE II extinction data using a regularized inversion technique. As the latter were observed to underestimate correlative in situ data of N and to overestimate correlative in situ values of R (Bingen et al., 2004a), the OE results can be considered the more realistic estimates.

– A comparison between vertical profiles of the OE and the PCA surface area densities (retrieved from the same SAGE II measurements) with correlative in situ data indicates that the Optimal

Estimation estimates of A tend to match the in situ values better than the Principal Component Analysis solutions of the operational SAGE II retrieval algorithm.

All these findings lead us to conclude that the new Optimal Estimation algorithm is able to significantly improve current estimates of aerosol microphysical properties retrieved from SAGE II satellite measurements in the volcanically unperturbed lower stratosphere.

A SAGE II climatology of monomodal aerosol properties generated by Steven Marsh using the new OE aerosol retrieval algorithm can be downloaded from http://www.atm.ox.ac.uk/project/PARTS/.

In the future, the algorithm can be adapted to other solar occultation instruments, like for instance SAGE III. As SAGE III has three additional aerosol channels the algorithm could be expanded to retrieve aerosol properties from bimodal particle size distributions, and consequently from volcanically enhanced aerosols.

Acknowledgements. We acknowledge the University of Canterbury and the Department of Physics and Astronomy for providing research funding in the form of a Doctoral Scholarship. The correlative in situ measurements above Wyoming have been obtained under support from a number of grants, primarily from the US National Science Foundation, and are available to the community at http://www-das.uwyo.edu/~deshler/. The SAGE II data were obtained from the NASA LaRC Atmospheric Science Data Center (ASDC).

References

Anderson, J., Brogniez, C., Cazier, L., Saxena, V. K., Lenoble, J., and McCormick, M.: Characterization of aerosols from simulated SAGE III measurements applying two retrieval techniques, J. Geophys. Res., 105, 2013–2027, 2000.

Arnold, F., Curtius, J., Spreng, S., and Deshler, T.: Stratospheric aerosol sulphuric acid: first direct in situ measurements using a novel ballonbased mass spectrometer apparatus, J. Atmos. Chem., 30, 3–10, 1998.

Barnes, J. E., and Hofmann, D. J.: Lidar measurements of stratospheric aerosol over Mauna Loa, Geophys. Res. Lett., 24, 1923–1926, 1997.

Bauman, J. J., Russel, P. B., Geller, M. A., and Hamill, P.: A stratospheric aerosol climatology from SAGE II and CLAES measurements: 1. Methodology, J. Geophys. Res, 108(D13), 4382, doi:10.1029/2002JD002992, 2003a.

Bauman, J. J., Russel, P. B., Geller, M. A., and Hamill, P.: A stratospheric aerosol climatology from SAGE II and CLAES measurements: 2. Results and comparisons, 1984–1999, J. Geophys. Res, 108(D13), 4383, doi:10.1029/2002JD002993, 2003b.

Bingen, C., Fussen, D., and Vanhellemont, F.: A global climatology of stratospheric aerosol size distribution parameters derived from SAGE II data over the period 1984–2000: 1. Methodology and climatological observations, J. Geophys. Res., 109, D06201, doi:10.1029/2003JD003518, 2004a.

Bingen, C., Fussen, D., and Vanhellemont, F.: A global climatology of stratospheric aerosol size distribution parameters derived from SAGE II data over the period 1984–2000: 2. Reference data, J. Geophys. Res., 109, D06202, doi:10.1029/2003JD003511, 2004b.

Chu, W. P., McCormick, M. P., Lenoble, J., Brogniez, C., and Pruvost, P.: SAGE II inversion algorithm, J. Geophys. Res., 94, 8339–8351, 1989.

Crutzen, P. J.: The influence of nitrogen oxide on the atmospheric ozone content, Q. J. R. Meteorol. Soc., 96, 320–327, 1970.

Crutzen, P. J.: The possible importance of CSO for the sulfate layer of the stratosphere, Geophys. Res. Lett., 3, 73–76, 1976.

Danilin, M. Y., Shia, R.-L., Ko, M. K. W., Weisenstein, D. K., Sze, N. D., Lamb, J. J., Smith, T. W., Lohn, P. D., and Prather, M. J.: Global stratospheric effects of the alumina emissions by solid-fueled rocket motors, J. Geophys. Res., 106, D12, 12 727–12 738, 2001.

Deshler, T., Hofmann, D. J., Johnson, B. J., and Rozier, W. R.: Balloonborne measurements of the Pinatubo aerosol size distribution and volatitlity at Laramie, Wyoming, during the summer of 1991, Geophys. Res. Lett., 19, 199–202, 1992.

Deshler, T., Hervig, M. E., Hofmann, D. J., Rosen, J. M., and Liley, J. B.: Thirty years of in situ stratospheric aerosol size distribution measurements from Laramie, Wyoming (41°N), using balloon-borne instruments, J. Geophys. Res., 108, 4167, doi:10.1029/2002JD002514, 2003.

Deshler, T., Anderson-Sprecher, R., Jäger, H., Barnes, J., Hofmann, D. J., Clemesha, B., Simonich, D., Osborn, M., Grainger, R. G., and Godin-Beekmann, S.: Trends in the nonvolcanic component of stratospheric aerosol over the period 1971 - 2004, J. Geophys. Res., 111, D01201, doi:10.1029/2005JD006089, 2006.

Deshler, T.: A Review of Global Stratospheric Aerosol: Measurements, Importance, Life Cycle, and Local Stratospheric Aerosol, Atmos. Res., 90, 223–232, 2008.

Deeter, M. N., Emmons, L. K., Francis, G. L., Edwards, D. P., Gille, J. C., Warner, J. X., Khattatov, B., Ziskin, D., Lamarque, J.-F., Ho, S.-P., Yudin, V., Attié, J.-L., Packman, D., Chen, J., Mao, D., and Drummond, J. R.: Operational carbon monoxide retrieval algorithm and selected results for the MOPITT instrument, J. Geophys. Res., 108, D14, 4399, doi:10.1029/2002JD003186, 2003.

Fahey, D. W., Kawa, S. R., Woodbridge, E. L., Tin, P., Wilson, J. C., Jonsson, H. H., Dye, J. E., Baumgardner, D., Borrmann, S., Toohey, D. W., Avallone, L. M., Proffitt, M. H., Margitan, J., Loewenstein, M., Podolske, J. R., Salawitch, R. J., Wofsy, S. C., Ko, M. K. W., Anderson, D. E., Schoeber, M. R., and Chan, K. R.: In situ measurements constrainting the role of sulphate aerosols in mid-latitude ozone depletion, Nature, 363, 509–514, doi:10.1038/363509a0, 1993.

Grainger, R. G.: The calculation of cloud parameters from AVHRR data, Ph.D. thesis, University of Auckland, New Zealand, 1990.

Grainger, R.G., Lambert, A., Taylor, F. W., Remedios, J. J., Rodgers, C. D., Corney, M., and Kerridge, B. J.: Infrared absorption by volcanic stratospheric aerosols observed by ISAMS, Geophys. Res. Lett., 20, 1283–1286, 1993.

Gruner, P. and H. Kleinert: Die Dämmerungserscheinungen, Probl. Kosm. Phys., 10, 1–113, 1927.

Hanson, D. R., and Lovejoy, E. R.: The reaction of $ClONO_2$ with submicrometer sulfuric acid aerosol, Science, 367, 1326–1328, 1995.

Heintzenberg, J., Müller, H., Quenzel, H., and Thomalla, E.: Information content of optical data with respect to aerosol properties: Numerical studies with a randomized minimization-search-technique inversion algorithm, Appl. Opt., 20, 1308–1315, 1981.

Hofmann, D. J., and Rosen, J. M.: Measurement of the sulfuric acid weight percent in the stratospheric aerosol from the El Chichón eruption, Geofisica Internacional, 23, 309–320, 1984.

Hofmann, D. J., Rosen, J. M., Pepin, T. J., and Pinnick, R. G.: Stratospheric aerosol measurements, I, Time variations at northern midlatitudes, J. Aatmos. Sci., 32, 1446–1456, 1975.

Jackman, C. H., Considine, D. B., and Fleming, E. L.: Space shuttle's impact on the stratosphere: an update, J. Geophys. Res., 101, D7, 12 523–12 529, 1996.

Jäger, H.: Long-term record of lidar observations of the stratospheric aerosol layer at Garmisch-Partenkirchen, J. Geophys. Res., 110, D08106, doi:10.1029/2004JD005506, 2005.

Junge, C. E., Changnon, C. W. and J. E. Manson: Stratospheric aerosols, J. Meteorol.,18, 81–108, 1961.

Kärcher, B., and Ström, J.: The roles of dynamical variability and aerosols in cirrus cloud formation, Atmos. Chem. Phys. Discuss., 3, 14151451, 2003.

Kjellstrom, E., Feichter, J., Sausen, R., and Hein, R.: The contribution of aircraft emissions to the atmospheric sulfur budget, Atmos. Environ., 33, 3455–3465, 1999.

McCormick, M. P., Hamill, P., Pepin, T. J., Chu, W. P., Swissler, T. J., and McMaster, L. R.: Satellite studies of the stratospheric aerosol, Bull. Am. Meteorol. Soc., 60, 1038–1046, 1979.

McCormick, M. P.: SAGE II: an overview, Adv. Space Res., 7, 219–226, 1987.

McCormick, M. P., Thomason, L. W. and C. R. Trepte : Atmospheric effects of the Mt. Pinatubo eruption, Nature, 373–399, 1995.

McMaster, L. R.: Stratospheric aerosol and gas experiment SAGE II, Am. Meteorol. Soc., Williamsburh, VA, paper presented at Sixth Conference on Atmospheric Radiation, 1986.

Mie, G.: Beiträge zur Optik trüber Medien speziell kolloidaler Metallösungen, Ann. Phys., 25, 377 pp., 1908.

Murphy, D. M., Thomson, D. S., and Mahoney, M. J.: In situ measurements of organics, meteoric material, mercury, and other elements in aerosols at 5 to 19 kilometers, Science, 282, 1664–1669, 1998.

Murphy, D. M., Cziczo, D. J., Hudson, P. K., and Thomson, D. S.: Carbonaceous material in aerosol particles in the lower stratosphere and tropopause region, J. Geophys. Res., 112, D04203, doi:10.1029/2006JD007297, 2007.

Osborn, M. R., DeCoursey, R. J., Trepte, C. R., Winder, D. M., and Woods, D. C.: Evolution of the Pinatubo volcanic cloud over Hampton, Virginia, Geophys. Res. Lett., 22, 1101–1104, 1995.

Palmer, K. F. and Williams, D.: Optical constants of sulfuric acid: application to the clouds of Venus?, Appl. Opt., 14, 208–219, 1975.

Penner, J. E., Chen, Y., Wang, M., and Liu, X.: Possible influence of anthropogenic aerosols on cirrus clouds and anthropogenic forcing, Atmos. Chem. Phys., 9, 879–896, 2009.

Pepin, T. J., McCormick, M. P., Chu, W. P., Simon, F., Swissler, T. J., Adams, R. R., Crumbly, K. R., and Fuller Jr., W. H.: Stratospheric aerosol measurements, NASA Spec. Publ., SP-421, 127–136, 1977.

Poole, L. R., and Pitts, M. C.: Polar stratospheric cloud climatology base on Stratospheric Aerosol Measurement II observations from 1978 to 1989, J. Geophys. Res., 99, 13 083–13 089, 1994.

Press, W. H., Teukolsky, S. A., Vetterling, W. T., and Flannery, B. P.: Numerical recipes in FORTRAN 77 – The art of scientific computing, Cambridge University Press, New York, USA, 2nd edn., 1992.

Pueschel, R. F.: Stratospheric aerosols: Formation, properties, effect, J. Aerosol Sci., 27, 383–402, 1996.

Rasch, P. J., Tilmes, S., Turco, R. P., Robock, A., Oman, L., Chen, C. C., Stenchikov, G. L., and Garcia, R. R.: An overview of geoengineering of climate using stratospheric sulphate aerosols, Phil. Trans. R. Soc., 366, 4007–4037, doi:10.1098/rsta.2008.0131, 2008.

Rasch, P. J., Crutzen, P., and Coleman, D. B.: Exploring the geoengineering of climate using stratospheric sulfate aerosols: The role of particle size, Geophys. Res. Lett., 35, L02809, doi:10.1029/2007GL032179, 2008.

Reeves, J. M., Wilson, J. C., Brock, C. A., and Bui, T. P.: Comparison of aerosol extinction coefficients, surface area density, and volume density from SAGE II and in situ aircraft measurements, J. Geophys. Res., 113, D10202, doi:10.1029/2007JD009357, 2008.

Renard, J.-B., Brogniez, C., Berthet, G., Bourgeois, Q., Gaubicher, B., Chartier, M., Balois, J.-Y., Verwaerde, C., Auriol, F., François, P., Daugeron, D., and Engrand, C.: Vertical distribution of the different types of aerosols in the stratosphere: Detection of solid particles and analysis of their spatial variability, J. Geophys. Res., 113, D21303, doi:10.1029/2008JD010150, 2008.

Rodgers, C. D.: Inverse methods for atmospheric sounding – Theory and practice, vol. 2 of *Atmospheric, Oceanic and Planetary Physics*, World Scientific, Singapore, 2000.

Rosen, J. M.: The boiling point of stratospheric aerosols, J. Appl. Meteor., 10, 1044–1046, 1971.

Russell, P. B. and Hamill, P.: Spatial variation of stratospheric aerosol acidity and model refractive index: Implications of recent results, J. Atmos. Sci., 41, 1781–1790, 1984.

Seinfeld, J. H., and Pandis, S. N.: Atmospheric chemistry and physics – from air pollution to climate change, Wiley & Sons, Inc., New York, 1998.

Semmler, M., Luo, B., and Koop, T.: Properties of ternary H_2SO_4-$(NH_4)_2SO_4$-H_2O at UT/LS conditions, in:

EGS – AGU – EUG Joint Assembly, EGU, Nice, France, Abstract No. 8691, 2003.

Sheridan, P. J., Schnell, R. C., Hofmann, D. J., and Deshler, T.: Electron microscope studies of Mt. Pinatubo aerosol layers over Laramie, Wyoming, during summer 1991, Geophys. Res. Lett., 19, 203–206, 1992.

Simonich, D. M., and Clemesha, B. R.: A history of aerosol measurements at São José dos Campos, Brazil (23° S, 46° W) from 1972–1995, Advances in Atmospheric Remote Sensing with Lidar - Selected papers of the 18. International Laser Radar Conference, Springer-Verlag, Berlin, Germany, 481–484, 1997.

Solomon, S.: Stratospheric ozone depletion: A review of concepts and theory, Rev. Geophys., 37, 275–316, 1999.

Steele, H. M. and Hamill, P.: Effects of temperature and humidity on the growth and optical properties of sulphuric acid-water droplets in the stratosphere, J. Aerosol Sci., 12, 517–528, 1981.

Steele, H. M. and Turco, R. P.: Retrieval of aerosol size distributions from satellite extinction spectra using constrained linear inversion, J. Geophys. Res., 102, 16737–16747, 1997.

Steele, H. M., Lumpe, J. D., Turco, R. P., Bevilacqua, R. M., and Massie, S. T.: Retrieval of aerosol surface area and volume densities from extinction measurements: Application to POAM II and SAGE II, J. Geophys. Res., 104, 9325–9336, 1999.

Talbot, R. W., Dibb, J. E., and Loomis, M. B.: Influences of vertical transport on free tropospheric aerosols over the central USA in springtime, Geophys. Res. Lett., 25, 1367–1370, 1998.

Taylor, J. R.: An introduction to Error Analysis, University Science Books, Sausalito, CA, Second Edition, 1939.

Thomason, L. W. and Poole, L. R.: Use of stratospheric aerosol properties as diagnostics of Antarctic vortex processes, J. Geophys. Res., 98, 23002–23012, 1993.

Thomason, L. W., Poole, L. R., and Deshler, T.: A global climatology of stratospheric aerosol surface area density deduced from Stratospheric Aerosol and Gas Experiment II measurements: 1984–1994, J. Geophys. Res., 102, D7, 8967–8976, 1997.

Thomason, L. W. and T. Peter (Eds.): Assessment of Stratospheric Aerosol Properties (ASAP), Stratospheric Processes and Their Role in Climate (SPARC), A project of the WMO/ICSU/IOC World Climate Research Programme, WCRP-124, WMO/TD-No. 1295, SPARC Report No. 4, 2006.

Thomason, L. W., Burton, S. P., Luo, B.-P., and Peter, T.: SAGE II measurements of stratospheric aerosol properties at non-volcanic levels, Atmos. Chem. Phys., 8, 983–995, 2008.

Tilmes, S., Garcia, R. R., Kinnison, D. E., Gettelman, A., and Rasch, P. J.: Impact of geoenineered aerosols on the troposphere and stratosphere, J. Geophys. Res., 114, D12305, doi:10.1029/2008JD011420, 2009.

Torres, O., Bhartia, P. K., Herman, J. R., Ahmad, Z., and Gleason, J.: Derivation of aerosol properties from satellite measurements of backscattered ultraviolet radiation: Theoretical basis, J. Geophys. Res., 103, D14, 17 099-17 110, 1998.

Trepte, C. R., and Hitchman, M. H.: Tropical stratospheric circulation deduced from satellite aerosol data, Nature, 355, 626–628, 1992.

Turco, R. P., Whitten, R. C., Toon, O. B., Pollack, J. B., and Hamill, P.: OCS, stratospheric aerosols and climate, Nature, 283, 283–386, 1980.

Wang, P. H., McCormick, M. P., Swissler, T. J., Osborn, M. T., Fuller, W. J., and Yue, G. K.: Inference of stratospheric aerosol composition and size distribution from SAGE II satellite measurements, J. Geophys.

Res., 94, 8435–8446, 1989.

Weisenstein, D., and Bekki, S.: Modeling of stratospheric aerosols, Chapter 6 of the SPARC assessment of stratospheric aerosol properties, In: Thomason, L. W., Peter, Th. (Eds.), WCRP-124, WMO/TD-No. 1295, SPARC Report No. 4, 2006.

Wurl, D.: Optimal Estimation Retrieval of Aerosol Microphysical Properties in the Lower Stratosphere from SAGE II Satellite Observations, Ph.D. thesis, University of Canterbury, New Zealand, 2008.

Tables

Table 1. Fractional contributions (in %) (to the total SAGE II spectral extinction at λ =[0.386, 0.452, 0.525, 1.020] µm) of particles smaller than 0.1 µm in the case of three normalized ($N = 0$) example background size distributions (**(a)** $R = 0.008$ µm, $S = 0.90$; **(b)** $R = 0.067$ µm, $S = 0.45$; **(c)** $R = 0.180$ µm, $S = 0.25$) and how they compare to typical SAGE II experimental uncertainties, $\sigma(\beta_\lambda)$.

R, S	$\Delta\beta$(0.386)	$\Delta\beta$(0.452)	$\Delta\beta$(0.525)	$\Delta\beta$(1.020)
0.008, 0.90	19	15	12	4
0.067, 0.45	15	13	11	6
0.180, 0.25	0.0	0.0	0.0	0.0
$\sigma(\beta_\lambda)$	10–60	5–35	3–25	1–10

Table 2. Fractional particle number, surface area density, and volume density (in %) of particles smaller than 0.1 µm in the case of three normalized ($N = 0$) example background size distributions **(a)** $R = 0.008$ µm, $S = 0.90$; **(b)** $R = 0.067$ µm, $S = 0.45$, and **(c)** $R = 0.180$ µm, $S = 0.25$.

R, S	ΔN	ΔA	ΔV
0.008, 0.90	99.7	83.3	52.5
0.067, 0.45	81.7	50.2	32.9
0.180, 0.25	0.8	0.2	0.1

Table 3. Model validation: Correlation coefficients, *cc*, describing the linear correlation between all accepted ("good") and the associated correct aerosol properties. Given the large number of measurements (≈230) these correlation coefficients are all significant at $p < 0.05\%$ (Taylor, 1939, Table C).

Retrieved vs True	*cc* (minNS)	*cc* (maxNS)
$\ln N$	0.56	0.52
$\ln R$	0.86	0.80
$\ln S$	0.85	0.70
$\ln A$	0.98	0.94
$\ln V$	1.00	0.98
$\ln R_{\mathrm{eff}}$	0.93	0.90

Table 4. Ensemble mean retrieved uncertainties (in %) in number density, median radius, distribution width, surface area density, volume density, and effective radius for both the minimum noise scenario (minNS) and the maximum noise scenario (maxNS).

Ens. Mean (%)	minNS	maxNS
σ_N, σ_R, σ_S	62, 24, 14	75, 37, 26
σ_A, σ_V, $\sigma_{\rm Reff}$	22, 11, 11	45, 34, 15

Table 5. Ensemble mean retrieved size distribution parameters (SAGE II data, December 1999) with associated uncertainties (in %). Number density is given in $\rm cm^{-3}$, median radius in µm, and lognormal distribution (half) width in log of µm.

SAGE II, Dec 1999	
N, R, S	
Ensemble Mean :	9.0, 0.069, 0.57
A priori:	4.7, 0.046, 0.48
σ_N, σ_R, σ_S (%)	
Ensemble Mean :	69, 33, 14
A priori:	93, 61, 31

Table 6. Ensemble mean retrieved surface area density, volume density, and effective radius (SAGE II data, December 1999) with associated uncertainties (in %). Surface area density is given in $\rm \mu m^2 cm^{-3}$, volume density in $\rm \mu m^3 cm^{-3}$, and effective radius in µm.

SAGE II, Dec 1999	
A, V, $R_{\rm eff}$	
Ensemble Mean :	1.00, 0.05, 0.16
A priori:	0.20, 0.005, 0.075
σ_A, σ_V, $\sigma_{\rm Reff}$ (%)	
Ensemble Mean :	23, 12, 13
A priori:	146, 179, 40

Table 7. Overview of uncertainties (in %) on aerosol properties retrieved under similar conditions (background aerosol, SAGE data) but using different retrieval techniques. The "+" indicates that the value is an estimate of partial errors only and that the total error is expected to be higher due to other disregarded uncertainty components. The uncertainties in A as reported by Steele et al. (1999) and Steele and Turco (1997), for instance, account for propagated random errors only. The total errors are expected to be higher by about 50% due to disregarded systematic (method bias) errors and contributions from particles smaller than $0.1\,\mu$m. The methods and the conditions under which these uncertainties were achieved are described in: (1) Wurl (2008), (2) Steele et al. (1999), (3) Thomason and Poole (1993), (4) Steele and Turco (1997), (5) Anderson et al. (2000), (6) Bingen et al. (2004b), (7) Wang et al. (1989), and (8) Bauman et al. (2003a). The acronyms stand for Principal Component Analysis (PCA), Constrained Linear Inversion (CLI), Randomized Minimization Search Technique (RMST), Regularized Inversion Method (RIM), Nonlinear Iterative Method (NIM), and Look-Up-Table approach (LUT).

Source/Method	σ_N	σ_R	σ_S	σ_A	σ_V	σ_{Reff}
(1)/OE	60–75	30–40	10–20	20–30	5–20	10–15
(2)/PCA				(15–20)+		
(3)/PCA				30	12–25	
(4)/CLI				25+	15+	15+
(5)/RMST				8–50	5–25	6–36
(6)/RIM	50–200	35–50	100–250			
(7)/NIM	<11	5–28				
(8)/LUT				20+	21+	18+

Figure Captions

Fig. 1. Histograms of number density **(a)**, median radius **(b)**, distribution width **(c)** as retrieved from synthetic aerosol extinction in the maximum noise scenario. The vertical lines indicate the a priori mean state (solid), and the a priori mean plus or minus one standard deviation (dash-dot).

Fig. 2. Histograms of surface area density **(a)**, volume density **(b)**, and effective radius **(c)** as derived from the retrieved distribution parameters shown in Fig. 1. The vertical line indicates the a priori mean state.

Fig. 3. Minimum Noise Scenario: True versus retrieved values of **(a)** particle number density N, **(b)** median radius R, **(c)** distribution width S, and **(d)** associated surface area density A, **(e)** volume density V, and **(f)** effective radius $R_{\rm eff}$, with their respective uncertainties. All values are given in $\log_{10}$. The broken line marks where the retrieved and true values are identical.

Fig. 4. As Fig. 3 but for the Maximum Noise Scenario.

Fig. 5. Histograms of 223 retrieved number densities **(a)**, median radii **(b)** and distribution width **(c)** as retrieved from synthetic aerosol extinction caused by background bimodal aerosols and large noise (maxNS). The vertical lines indicate the a priori mean state (solid), and the a priori mean state plus or minus one standard deviation (dash-dot).

Fig. 6. As Fig. 5 but for the resulting integrated aerosol properties, surface area density **(a)**, volume density **(b)** and effective radius **(c)**. The vertical line indicates the a priori mean state (solid).

Fig. 7. Integrated monomodal aerosol properties as retrieved from bimodal background aerosol in comparison with the correct bimodal surface area densities **(a)**, volume density **(b)** and effective radius **(c)**. The linear correlation coefficients are 0.87 in A, 0.96 in V and 0.38 in $R_{\rm eff}$ (significant at $p > 0.05\%$, Taylor (1939, Table C).

Fig. 8. Histograms of number density **(a)**, median radius **(b)**, distribution width **(c)** as retrieved from SAGE II measurements of aerosol extinction in December 1999. The vertical lines indicate the a priori mean state (solid), and the a priori mean state plus or minus one standard deviation (dash-dot).

Fig. 9. Histograms of surface area density **(a)**, volume density **(b)**, effective radius **(c)** as derived from the retrieved size distribution parameters shown in Fig. 8. The vertical lines indicate the a priori mean.

Fig. 10. SAGE II, 12/1999: Histograms of the retrieved uncertainties (in %) in number density N, median particle radius R, and distribution width S.

Fig. 11. SAGE II, 12/1999: Histograms of the uncertainties (in %) associated with surface area density **(a)**, volume density **(b)**, and effective radius **(c)**.

Fig. 12. SAGE II measurements (December 1999): Principal Component Analysis (PCA) retrieval results of surface area density in $\mu m^2\,cm^{-3}$, effective radius $R_{\rm eff}$ in µm (courtesy of NASA LaRC) and the associated volume density in $\mu m^3\,cm^{-3}$, compared to the Optimal Estimation retrieval results. The diagonal line marks $x = y$ where both results would be identical.

Fig. 13. Difference (in %) between the retrieved Optimal Estimation surface area densities (A), volume densities (V), and effective radii ($R_{\rm eff}$) and the Principal Component Analysis (PCA) results: (PCA-OE)/OE. Frames **(a–c)**: Difference as a function of A, V, $R_{\rm eff}$. Frames **(d–f)**: Cumulative histograms of the differences.

Fig. 14. Vertical profiles of surface area density. Frames **(a)**/**(c)**/**(e)**/**(g)**: Surface areas as retrieved (from SAGE data) by the NASA LaRC using the PCA approach (diamonds with error bars, measured on 22 June (a), 23 June (c), 14 December (e) and 16 December 1999 (g)) and correlative in situ (OPC) measurements (without error bars, measured on 23 June and 10 December 1999); the vertical dashed line marks the a priori mean, and the short horizontal dotted line marks the tropopause level (NMC data) at the time of the SAGE II measurements. Frames **(b)**/**(d)**/**(f)**/**(h)**: Associated relative differences. The long vertical lines mark the zero (solid) and the profile mean difference (dotted). The a priori uncertainty of 40% (Deshler et al., 2003) is marked by the dash-dotted line.

Fig. 15. As Fig. 14 but for surface area density as derived from the retrieved Optimal Estimation size distribution parameters.

Fig. 16. Locations of SAGE II measurement events in March, June, September, and December 1999. The square marks the approximate location of Laramie/Wyoming (41° N, 105° W)

Fig. 17. Number of measurements per 10° latitude and 1 km altitude grid box. Each grid box is represented by a spot. Contours are marked for 10, 50, 100, 200, and 300 counts.

Fig. 18. Histograms of number density **(a)**, median radius **(b)**, distribution width **(c)** as retrieved from SAGE II measurements of aerosol extinction in September 1999. The vertical lines indicate the a priori mean state (solid), and the a priori mean state plus or minus one standard deviation (dash-dot).

Figures

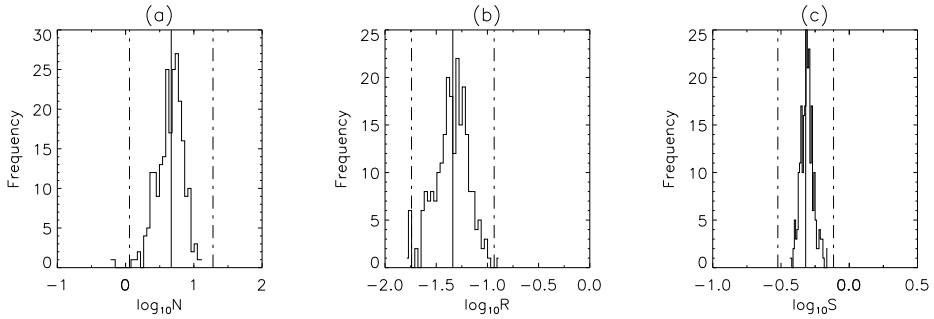

Fig. 1. Histograms of number density **(a)**, median radius **(b)**, distribution width **(c)** as retrieved from synthetic aerosol extinction in the maximum noise scenario. The vertical lines indicate the a priori mean state (solid), and the a priori mean plus or minus one standard deviation (dash-dot).

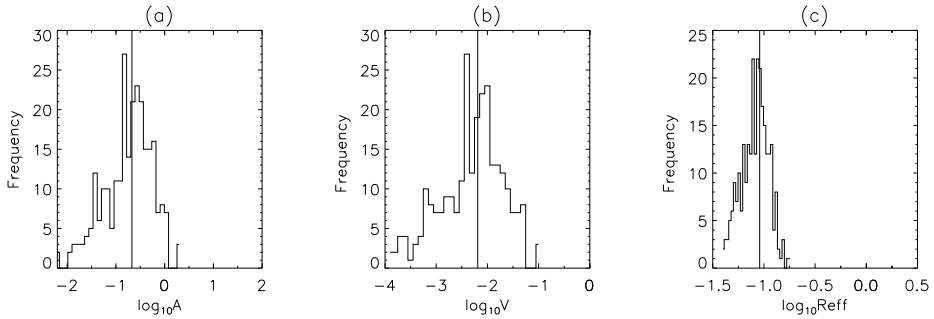

Fig. 2. Histograms of surface area density **(a)**, volume density **(b)**, and effective radius **(c)** as derived from the retrieved distribution parameters shown in Fig. 1. The vertical line indicates the a priori mean state.

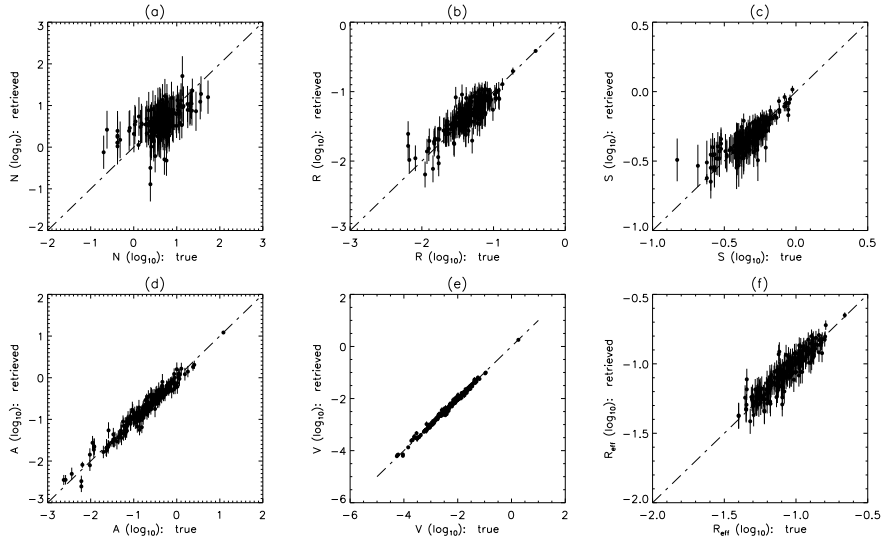

Fig. 3. Minimum Noise Scenario: True versus retrieved values of **(a)** particle number density N, **(b)** median radius R, **(c)** distribution width S, and **(d)** associated surface area density A, **(e)** volume density V, and **(f)** effective radius $R_{\rm eff}$, with their respective uncertainties. All values are given in $\log_{10}$. The broken line marks where the retrieved and true values are identical.

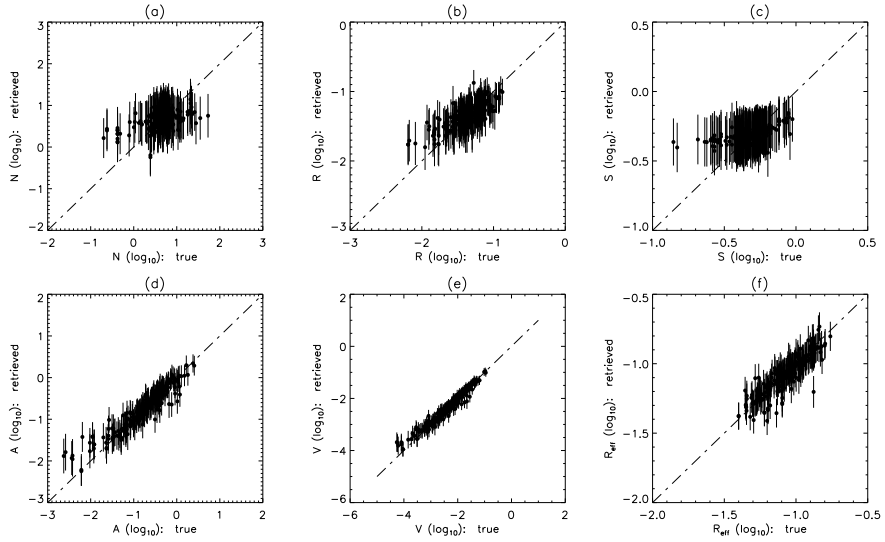

Fig. 4. As Fig. 3 but for the Maximum Noise Scenario.

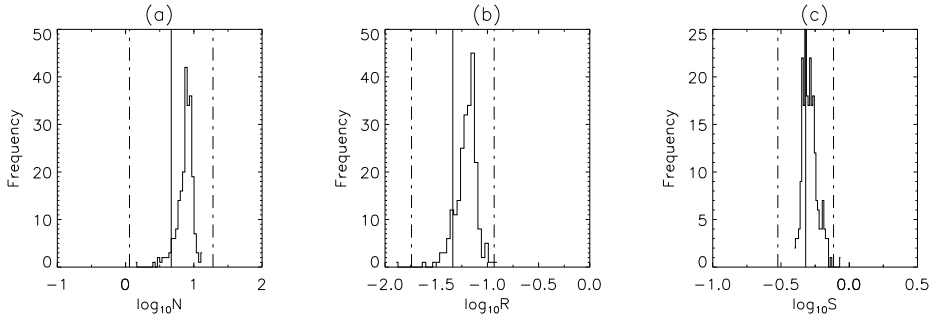

Fig. 5. Histograms of 223 retrieved number densities **(a)**, median radii **(b)** and distribution width **(c)** as retrieved from synthetic aerosol extinction caused by background bimodal aerosols and large noise (maxNS). The vertical lines indicate the a priori mean state (solid), and the a priori mean state plus or minus one standard deviation (dash-dot).

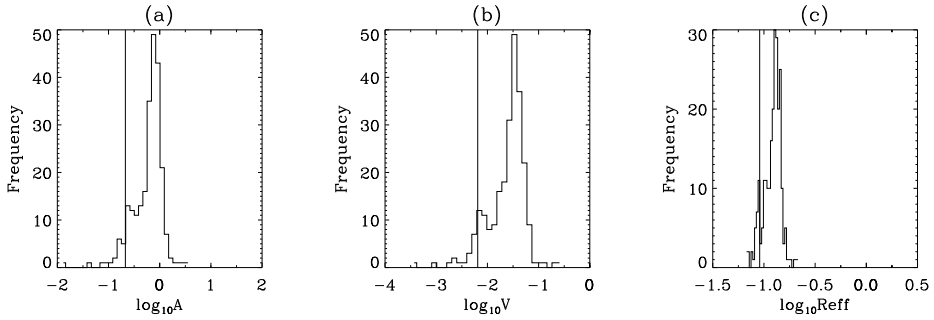

Fig. 6. As Fig. 5 but for the resulting integrated aerosol properties, surface area density **(a)**, volume density **(b)** and effective radius **(c)**. The vertical line indicates the a priori mean state (solid).

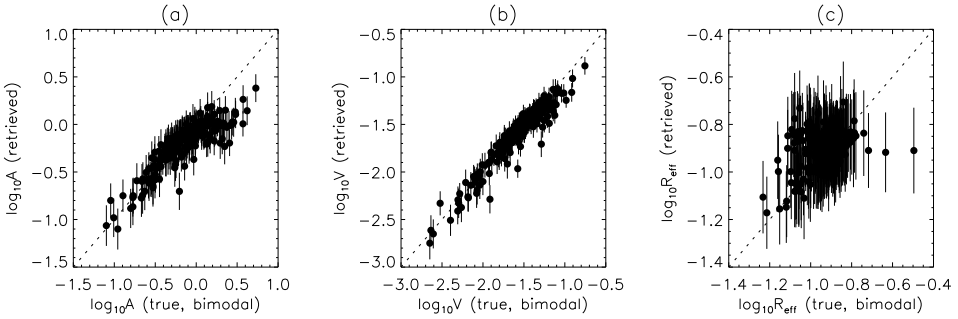

Fig. 7. Integrated monomodal aerosol properties as retrieved from bimodal background aerosol in comparison with the correct bimodal surface area densities **(a)**, volume density **(b)** and effective radius **(c)**. The linear correlation coefficients are 0.87 in A, 0.96 in V and 0.38 in R_{eff} (significant at $p > 0.05\%$, Taylor (1939, Table C).

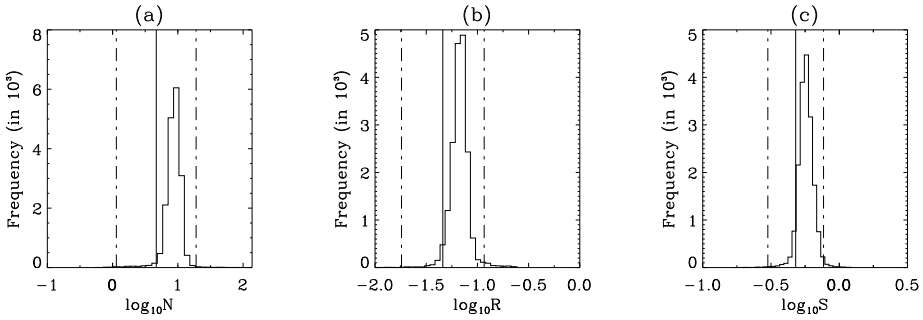

Fig. 8. Histograms of number density **(a)**, median radius **(b)**, distribution width **(c)** as retrieved from SAGE II measurements of aerosol extinction in December 1999. The vertical lines indicate the a priori mean state (solid), and the a priori mean state plus or minus one standard deviation (dash-dot).

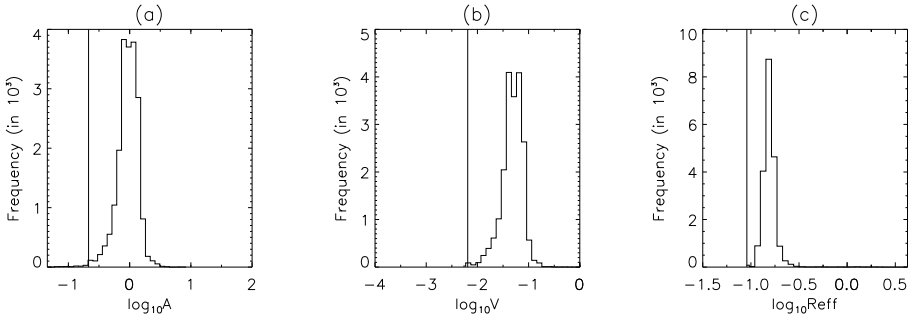

Fig. 9. Histograms of surface area density **(a)**, volume density **(b)**, effective radius **(c)** as derived from the retrieved size distribution parameters shown in Fig. 8. The vertical lines indicate the a priori mean.

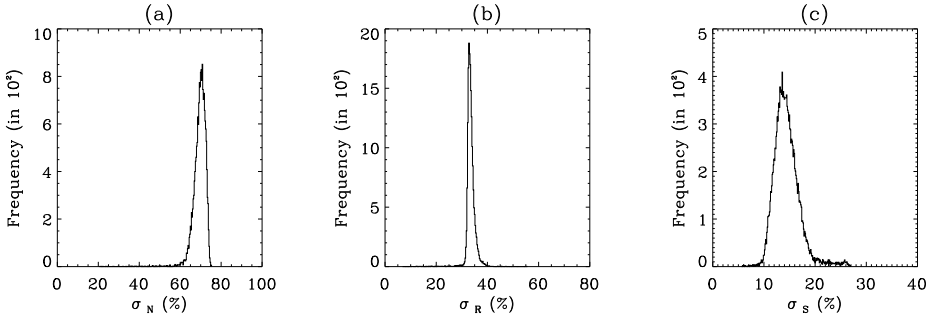

Fig. 10. SAGE II, 12/1999: Histograms of the retrieved uncertainties (in %) in number density N, median particle radius R, and distribution width S.

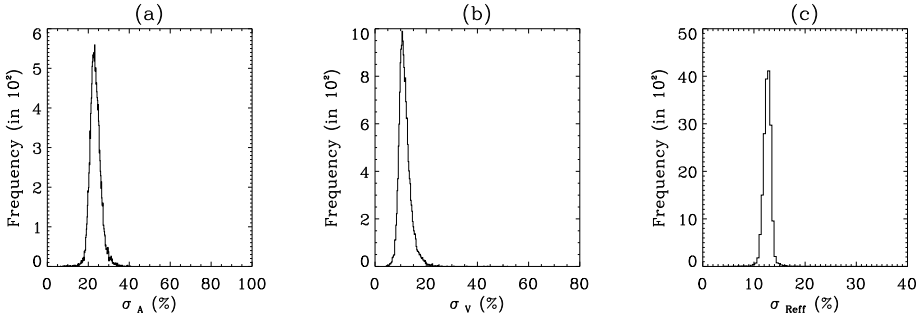

Fig. 11. SAGE II, 12/1999: Histograms of the uncertainties (in %) associated with surface area density **(a)**, volume density **(b)**, and effective radius **(c)**.

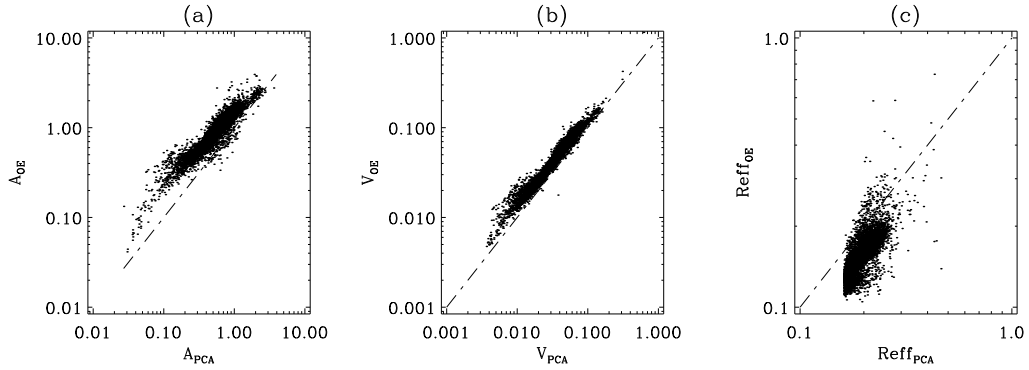

Fig. 12. SAGE II measurements (December 1999): Principal Component Analysis (PCA) retrieval results of surface area density in $\mu m^2\,cm^{-3}$, effective radius $R_{\rm eff}$ in µm (courtesy of NASA LaRC) and the associated volume density in $\mu m^3\,cm^{-3}$, compared to the Optimal Estimation retrieval results. The diagonal line marks $x = y$ where both results would be identical.

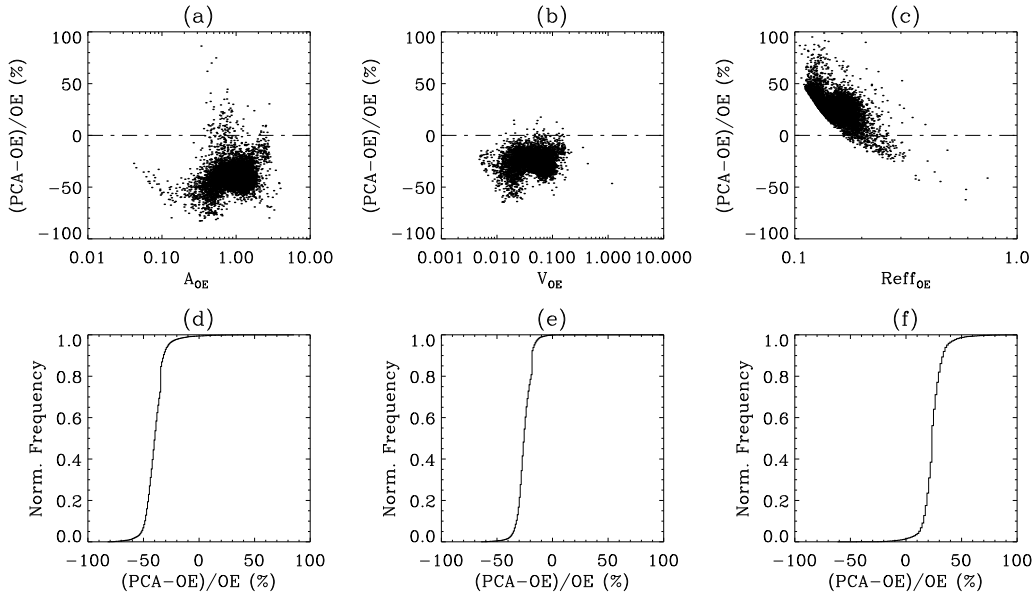

Fig. 13. Difference (in %) between the retrieved Optimal Estimation surface area densities (A), volume densities (V), and effective radii ($R_{\rm eff}$) and the Principal Component Analysis (PCA) results: (PCA-OE)/OE. Frames **(a–c)**: Difference as a function of A, V, $R_{\rm eff}$. Frames **(d–f)**: Cumulative histograms of the differences.

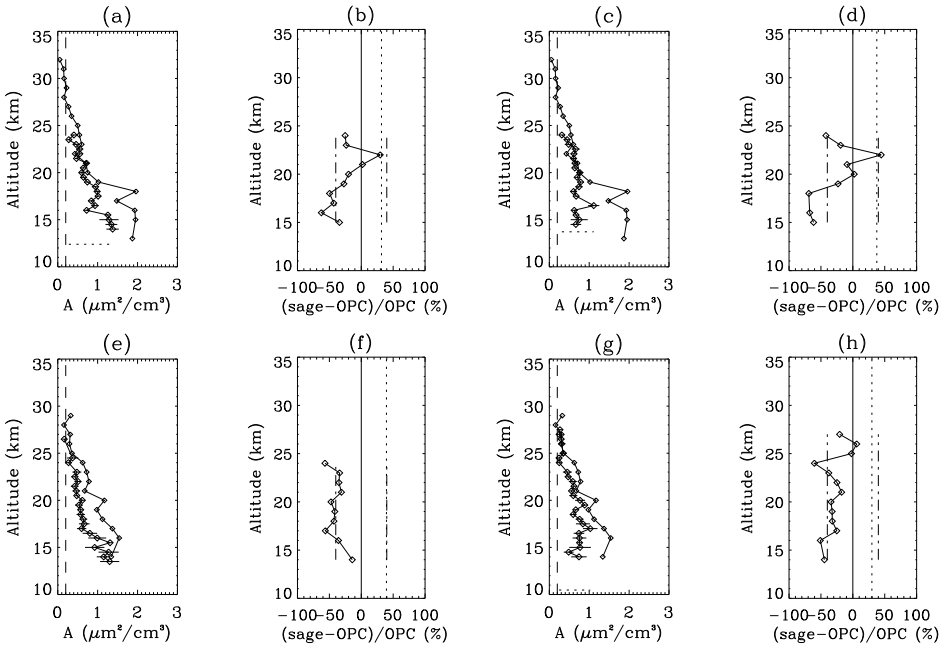

Fig. 14. Vertical profiles of surface area density. Frames **(a)**/**(c)**/**(e)**/**(g)**: Surface areas as retrieved (from SAGE data) by the NASA LaRC using the PCA approach (diamonds with error bars, measured on 22 June (a), 23 June (c), 14 December (e) and 16 December 1999 (g)) and correlative in situ (OPC) measurements (without error bars, measured on 23 June and 10 December 1999); the vertical dashed line marks the a priori mean, and the short horizontal dotted line marks the tropopause level (NMC data) at the time of the SAGE II measurements. Frames **(b)**/**(d)**/**(f)**/**(h)**: Associated relative differences. The long vertical lines mark the zero (solid) and the profile mean difference (dotted). The a priori uncertainty of 40% (Deshler et al., 2003) is marked by the dash-dotted line.

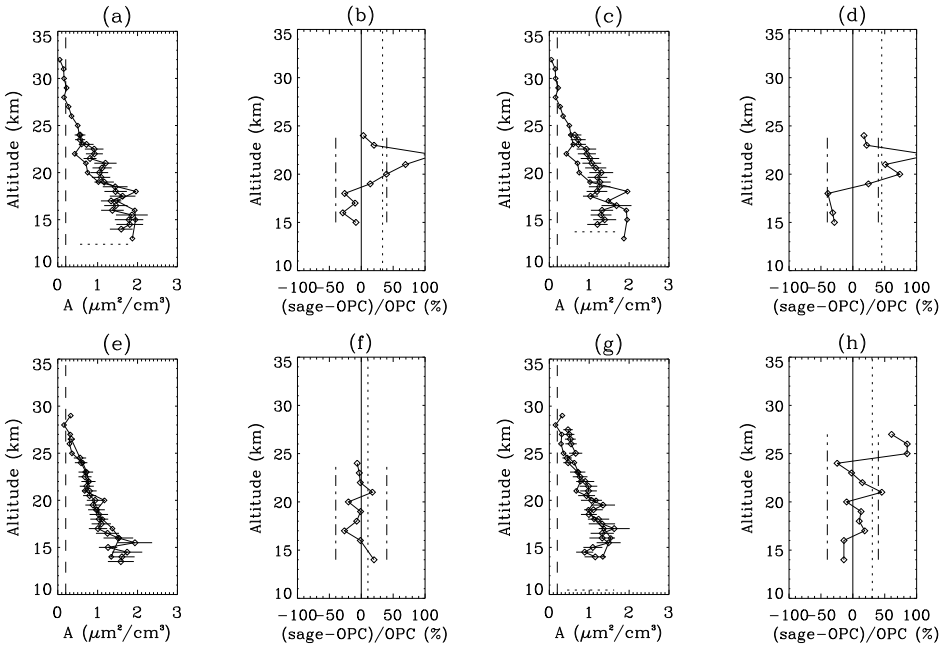

Fig. 15. As Fig. 14 but for surface area density as derived from the retrieved Optimal Estimation size distribution parameters.

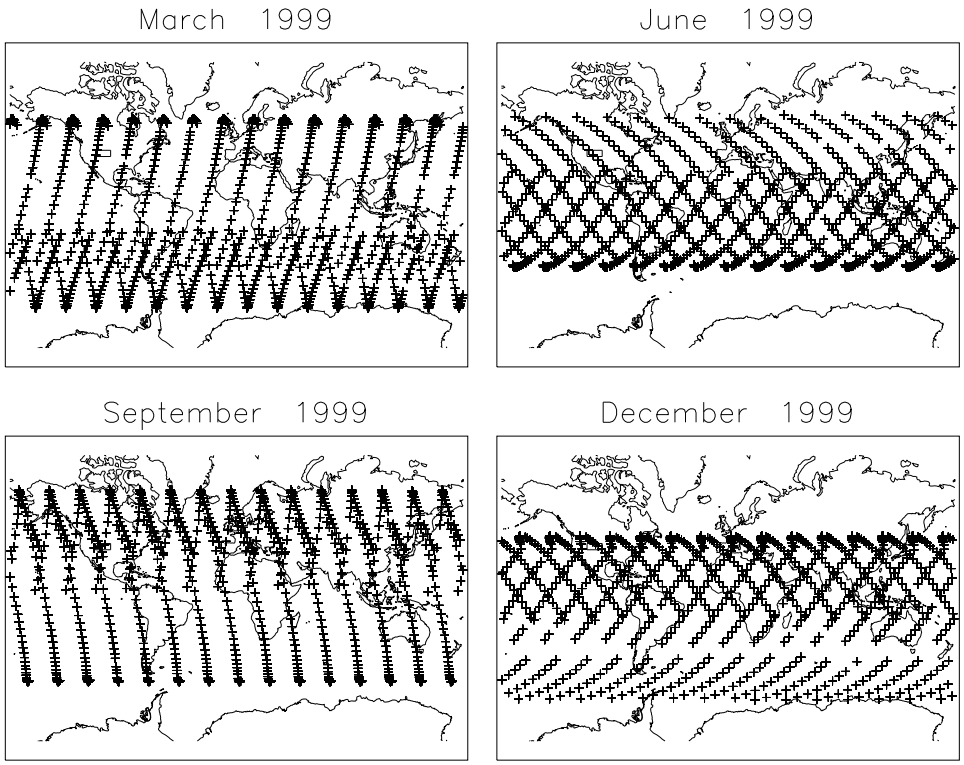

Fig. 16. Locations of SAGE II measurement events in March, June, September, and December 1999. The square marks the approximate location of Laramie/Wyoming (41° N, 105° W)

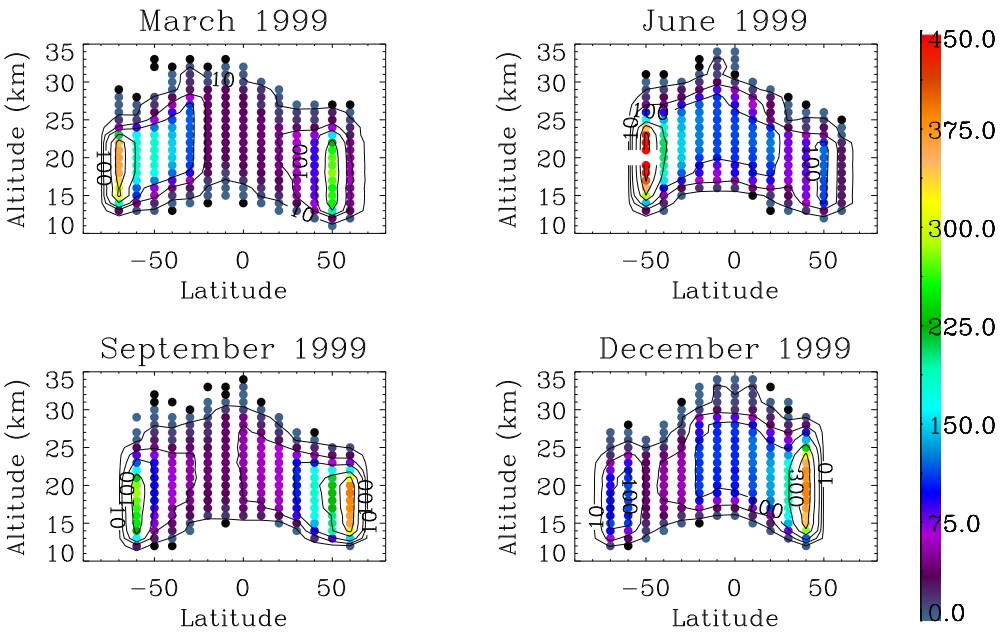

Fig. 17. Number of measurements per 10° latitude and 1 km altitude grid box. Each grid box is represented by a spot. Contours are marked for 10, 50, 100, 200, and 300 counts.

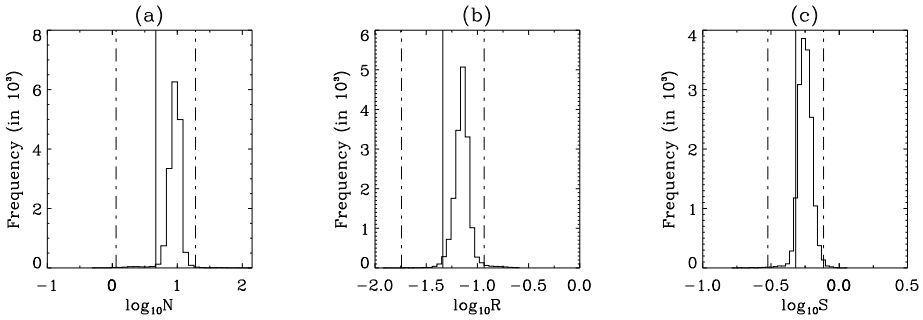

Fig. 18. Histograms of number density **(a)**, median radius **(b)**, distribution width **(c)** as retrieved from SAGE II measurements of aerosol extinction in September 1999. The vertical lines indicate the a priori mean state (solid), and the a priori mean state plus or minus one standard deviation (dash-dot).